This manuscript has been published by the Journal of Constructional Steel Research 2020, Vol. 166, pp. 105907.
doi.org/10.1016/j.jcsr.2019.105907

Full-range behaviour of double web angle connections

Shen Yan, Luli Jiang and Kim J.R. Rasmussen

University of Sydney, School of Civil Engineering, Sydney, Australia

Abstract: This paper presents recent experimental and analytical investigations on the full-range flexural behaviour of double web angle connections. Experiments were carried out on bolted double web angle connections with two different configurations featuring three and five bolt rows, respectively. For each connection configuration, five nominally identical specimens were tested to investigate the variability of connection behaviour, including joint stiffness, ultimate resistance and ductility, thereby making a total of ten tests. All tests were conducted well into the post-ultimate range until complete failure of the connection, examining the full-range connection response. The load transferring mechanism of the connection was dynamically changing, partly because the presence of bolt hole clearance caused certain bolts to be initially inactive, only to later become active in transferring load from the beam, and partly because when the beam bottom flange came into contact with the column flange under large connection rotation, the centre of rotation changed causing the compressive load transferred at the bottom bolt rows to unload and reverse. To capture the above complicated changes of load transferring mechanisms and thus capture the full-range behaviour of a bolted web angle connection, an advanced mechanical model was proposed. The model is based on the Component Method, and adopts a decision tree to track the evolution of the load-transferring mechanism of the connection, including the bearing state of each bolt, either under tensile or compressive load, the potential presence of contact between the beam bottom flange and the column flange, and the plastic deformation of the critical connection components. The proposed model was applied to the tested connections with excellent agreement observed between the model predictions and the experimental results. Not only producing full-range force-displacement curves that are very

This manuscript has been published by the Journal of Constructional Steel Research 2020, Vol. 166, pp. 105907.
doi.org/10.1016/j.jcsr.2019.105907

close to the experimental curves, the proposed model also provides useful information about the internal state of the connection, which was not obtainable from the tests.

Keywords: Web angle connection; experimental investigation; full-range behaviour; component method

1. Introduction

The bolted web angle connection is among the most popular connection types used in steel construction, mainly because of its low labour costs. In structural analysis and design, a web angle connection is normally simplified as a perfectly pinned joint, but in practice, it shows semi-rigid flexural behaviour [1]. Considering connection semi-rigidity directly affects the strength and serviceability of unbraced steel frames, the flexural behaviour of web angle connections has been extensively examined through experimental investigations, including those in [2-7]. Moreover, analytical models were proposed to predict the connection flexural response, primarily the initial stiffness and ultimate strength [5, 8-12].

Despite the existing large number of studies, several important issues remain unaddressed. Firstly, the available experimental studies mainly dealt with initial stiffness and strength of connections, while few focused on the full-range behaviour, including gradual yielding of components, ultimate limit states involving fracture, and post-ultimate response characterised by fracture propagation. The full-range behaviour of connections may seem of less interest in conventional structural design, but is becoming increasingly important because the ongoing trends towards adopting performance-based design and designing by advanced analysis require knowledge of the full-range behaviour of members and connections [13]. Secondly, while variability in material properties has been thoroughly researched, little is known about the variability in connection behaviour, which also results from randomness in geometrical properties and fabrication imperfections. It has been pointed out that the uncertainty in connection behaviour significantly affects the evaluation of reliability of steel frames [14]. Tests on nominally identical specimens are indispensable in examining the variability in connection properties, but have been seldomly reported. Thirdly, the available connection models for web angle connections are empirical or semi-mechanical, and thus proved to be accurate only for certain limited range of connection geometries [1]. The Component Method as a pure mechanical method [15], however, has not been applied to the web angle connection. To the authors' knowledge, this is likely because the behaviour of a web angle connection cannot be accurately modelled within the conventional Component Method framework, as the connection behaviour features transitions between different load-transferring mechanisms, involving changes in bolt bearing states resulting from initial bolt hole clearance and contact between the beam bottom flange and the column flange under large rotations.

This paper presents a study aimed at addressing the above mentioned issues. A total of ten web angle connections with two connection configurations were tested, with each configuration having five nominally identical specimens so as to evaluate the variability in connection behaviour. All connections were loaded well into the post-ultimate range, investigating the full-range connection behaviour, including initial stiffness, gradual yielding, ultimate bending strength, ductility and fracture. A component-based mechanical model is proposed for web angle connections to predict the full-range connection behaviour. The model tracks the progressively changing load-transferring mechanism of the connection, and thus is capable of capturing the bearing state of each bolt, either under tensile or compressive load, the contact state between beam bottom flange and column flange, the plastic deformation of the critical connection components, and the progressive propagation of fracture in the connection. The proposed model is shown to be in excellent agreement with the experimental results.

2. Experimental program

2.1 Specimen details

Two connection configurations were studied, referred to as WA360 and WA460. The configurations are different in terms of beam size, angle cleat length and number of bolt rows on the angle cleats, as shown in Fig. 1. For each connection configuration, five nominally identical specimens (WA360-1 to WA360-5, and, WA460-1 to WA460-5) were tested to determine the statistical characteristic of variability in connection behaviour.

The WA360 and WA460 connections used 360 UB 56.7 and 460 UB 82.1 beams, respectively. The beams had a length of 1000 mm between the beam end facing the column and the loading point at the other end. The gap between the beam end and the column flange was 20 mm. The columns used in all experiments were 250UC89.5, and had pinned supports at both ends spaced 1200 mm apart. A pair of 100x100x8EA angle cleats were used to connect the beam web to the column flange with one angle on each side of the beam web. The bolts were M20 (Grade 10.9) [16]. In the WA360 connections, the angle cleats were 210 mm in length and had 3 bolt rows, while in the WA460 connections, the angles were 350 mm in length and had 5 bolt rows. An identical spacing of 70 mm between neighboring bolt rows was used for both connection configurations. The bolts were designed as snug tight bolts, and had sufficient strength to transfer the applied loads beyond the

84 ultimate resistance of the connections, thus avoiding catastrophic bolt shear failure without noticeable
85 deformation. The bolt holes in the beam web and in the angle cleats had a diameter of 22 mm, producing a 2
86 mm bolt hole clearance in accordance with AISC 360 [17].

87 Beams, columns and angle cleats were all manufactured from AS 300 grade steel to AS/NZS3679.1 [18].
88 Tests were undertaken on standard tensile coupons. The tests were paused for 100 s every 10-15 mins after the
89 commencement of yielding so as to obtain the static material properties. For each section, two coupons were
90 tested and the results were averaged. The angle cleats were hot-rolled, and the stress vs. strain curves showed a
91 sharp elasticity-to-plasticity transition. Table 2 summaries the material properties.

92

93 ## 2.2 Test setup, instrumentation and procedure

94 Figure 2(a) shows the test setup. The column was positioned horizontally and pin-supported at each end.
95 One support had circular holes while the other had slotted holes, producing a simply supported condition for
96 the column. At the bottom surfaces, the supports were bolted to the base beam, which was firmly bolted to the
97 floor to avoid out-of-plane overturning. The beam was upright and loaded at the end by a servo-controlled
98 hydraulic jack through a loading arm. The loading arm was pin-connected to the beam end and the hydraulic
99 jack, thereby transferring axial load only.

100 Figure 2(b) shows the experimental instrumentation. Load applied from the hydraulic jack, F, was monitored
101 using a load cell connected to the jack. Rotations of the beam were measured at three locations, θ_{BT}, θ_{TM}, θ_{BB},
102 using three inclinometers attached to the beam, i.e., I-1, I-2, I-3, respectively. Inclinometers I-1 and I-2 were
103 mounted on the web of the beam, while Inclinometer I-3 was mounted on a thin plate tack-welded to the tensile
104 flange of the beam. Rotation of the loading arm, θ_{LA}, was measured using Inclinometer I-4 attached on the
105 surface of the loading arm. These rotations were assumed positive when the beam or the loading arm rotated
106 clockwise, and negative when rotating counterclockwise. Two displacement transducers (LVDTs), DT-1 and
107 DT-2, were placed between the column flanges, close to the column web. They registered perpendicularly
108 against the inner surface of the top column flange, and were aligned to the flanges of the beam, with DT-1
109 aligned to the tensile flange and DT-2 aligned to the compressive flange. The measurements of Displacement

Transducers DT-1 and DT-2 were δ_{DT1} and δ_{DT1}, respectively, which were assumed positive when the column flange deflected upwards, and were negative otherwise.

Allowed to have free rotation at both ends, the loading arm tilted as the beam rotated. With a rotation of the loading arm of θ_{LA}, the load transferred to the beam end, F_{LA}, was equal to F / cos(θ_{LA}). Thus, the bending moment acting at the intersection between the centerlines of the beam and column, M, was:

$$M = \frac{\cos\left(\theta_{BT} - \theta_{LA}\right)}{\cos(\theta_{LA})} \cdot FL \tag{1}$$

where L is the distance between the transfer pin on the beam top end and the centerline of the column, and was equal to 1145 mm in all tests. The rotations of the beam and loading arm also induced an axial force in the beam, equal to:

$$N = \frac{\sin\left(\theta_{BT} - \theta_{LA}\right)}{\cos(\theta_{LA})} \cdot F \tag{2}$$

The connection rotation, θ, is defined as the relative rotation between the bottom part of the beam and the centerline of the column. Localised deformations of the column were assumed to be negligible so that the rotation of the column centerline was equal to the rotation of the top flange. Thus, θ was calculated as:

$$\theta = \theta_{BB} - \arctan\left(\frac{\delta_{DT1} - \delta_{DT2}}{h_B}\right) \tag{3}$$

where h_B is the beam depth.

All specimens were tested following the same procedure. The hydraulic jack applied load in a displacement-control mode with a loading rate of 1 mm/min up to the occurrence of the first fracture, which was usually associated with a dramatic drop in load. Subsequently, the loading rate was increased to 10 mm/min until the complete failure of the connection. During the whole loading course, all data were recorded at 1 sec intervals. Due to strain rate effect, the measured resistance of a connection in the test is normally higher than the static resistance, as has been observed in the previous tests [13]. Therefore, every 20-30 min, the test was paused for 2 mins to achieve full stress relaxation and thus obtain the static resistance. The full-range static resistance curve was obtained by fitting a smooth curve through the static resistance measurement points. It was observed that the strain rate effect caused an approximately 2% increase in the connection resistance in this experimental program.

3. Experimental results

3.1 WA360 tests

Figure 3 shows the test results of specimen WA360-1, including the moment-rotation curve and a selection of pictures illustrating experimental phenomena at different stages of loading. When the loading started, the connection performed linearly with a large bending stiffness, reaching a bending moment of 10.6 kN·m at a rotation of 0.0023 rad, which is marked by Point A on the moment-rotation curve. During this linear stage, the bending resistance resulted from the force couple of the static friction forces at the bolts connecting the beam web to the angle cleats. At Point A, the static friction forces at the bolts were overcome, and the bolts started to slip due to the existence of the 2-mm initial clearance of the bolt holes. Slip of bolts stopped at Point B when effective bearing was established between the bolts and the bolt holes in the beam web and in the angle cleats. During bolt slip stage, the kinetic friction was largely constant in magnitude, leading to a plateau on the moment-rotation curve between Points A and B, with Point B featuring a bending moment of 9.99 kN·m at a rotation of 0.020 rad.

Subsequently, the top and bottom bolt rows started to transfer tensile and compressive loads, respectively, through bearing of bolts, and the moment resistance of the connection increased notably. The increase in resistance is nonlinear due to the gradual yielding of the angle cleats and the edge of bolt holes in the beam web. The middle bolt row had a smaller distance to the centre of rotation of the joint, so bearing at the middle bolt row started later than bearing at the top and bottom bolt rows. The instrumentation did not allow the exact point of loading at which bearing started to be determined. However, the component-based mechanical model proposed in Section 4 gives an insight to the bearing state of each bolt as the loading increased.

At a rotation of 0.146 rad, i.e. Point C on the moment-rotation curve, the compressive flange of the beam came into contact with the face of the column flange. The beam-to-column contact produced high compressive stiffness, causing the contact point to become the new centre of compression of the joint, and increasing the lever arm between the parts of the connection transferring compression and tension. Hence, the moment resistance and the joint stiffness increased dramatically from Point C onward. As the joint started to rotate about the beam-to-column contact point, the compressive load transferred through the bottom bolt row started to

unload. After the unloading finished, no load was transferred through the bottom bolt for a time period due to the clearance of the bolt hole. Then, as the joint rotation increased further, the bottom bolt started to bear against the bolt holes again, but now transferring tensile load from the beam web. The exact points of loading when the abovementioned changes of the bolt bearing state occurred were not observable in the tests, but could be determined from the mechanical model proposed in Section 4. From Point C onward, the plastic deformation of the web angle developed significantly, as shown by Point D in Fig. 3.

As the load was further increased, fracture initiated near the root of the angle segment aligning with the top bolt row, and quickly propagated towards the tensile edge of the angle cleat, leading to a significant reduction in stiffness. The ultimate bending resistance was reached soon after at Point E. Subsequently, the crack propagated towards the compressive edge of the angle cleat, resulting in a significant reduction in bending resistance. This progressive fracture led to the final failure of the connection, shown as Point F in Fig. 3. The connection was disassembled after the test to investigate the plastic deformations of the component parts. At the top and bottom bolt rows, significant plastic deformation was observed at the bolt hole edge on the beam-end side, with the plastic deformation at the top bolt hole appreciably larger than at the bottom hole. At the bottom bolt row, plastic deformation was observed at the bolt hole edge on both sides, which was evidence of the transition between bolt bearing states at the bottom bolt row.

The loading scheme adopted in this experimental program generated a small amount of axial tension in the beam, due to the rotations of the beam and loading arm. The axial tensile force increased with increasing applied load, and had a maximum value of 20.6 kN which accounted for only 0.9% of the plastic axial resistance of the beam. Assuming the axial force was evenly transferred through the three bolts, each bolt was subjected to an additional tensile load of 6.9 kN as a result of the induced tensile force. By comparison, the bending moment generated a tensile load of 202 kN in the bolt of the top bolt row where failure of the connection initiated (this value was not obtainable from the test, and thus was calculated using the mechanical model in Section 4). Therefore, the effect of the axial tensile force was negligible when compared to the effect of the bending moment.

The other nominally identical WA360 specimens behaved similarly to Specimen WA360-1, with the moment-rotation curves featuring an initial linear range, a plateau of varying length, a nonlinear response associated with plastic deformation of the angle cleats, a hardening range resulting from contact between the

beam compressive flange and column flange, and a post-ultimate range due to progressive fracture of the angle cleats along the root, as shown in Fig. 4. Although all specimens were nominally identical, certain variations in response were observed, primarily including: *a*) initial stiffness, from 2830 kN·m/rad (WA360-2) to 4550 kN·m/rad (WA360-1); *b*) limit of the initial linear stage, from 3.90 kN·m (WA360-2) to 12.6 kN·m (WA360-5); *c*) rotation at which bolts stopped slipping, from 0.0197 (WA360-1) rad to 0.0415 rad (WA360-3); *d*) resistance when beam-to-column contact occurred, from 30.0 kN·m (WA360-4) to 33.7 kN·m (WA360-1); *e*) rotation when beam-to-column contact occurred, from 0.135 rad (WA360-4) to 0.146 rad (WA360-1); *f*) ultimate bending resistance, from 87.3 kN·m (WA360-3) to 101 kN·m (WA360-2); *g*) joint rotation corresponding to the ultimate resistance, from 0.250 rad (WA360-4) to 0.308 (WA360-2); and *h*) joint ductility, determined as the joint rotation when the resistance decreases to 10 kN·m (about 10% of the ultimate strength), from 0.350 rad (WA360-4) to 0.511 rad (WA360-5).

Table 2 summarises the results of all WA360 tests. Statistical values of the above joint responses are also presented in the Table. Resistances of the initial linear stage and the end of the bolt slip stage were highly variable, with CoVs as high as 0.533 and 0.288, respectively. The variability is attributed to the use of snug tight bolts which implied a high degree of variability in the pre-tension forces induced during tightening. Due to random imperfections in fabrication, joint rotation at the end of the bolt slip stage also showed relatively large variability, with a CoV of 0.318. Responses of different connections following the bolt slip stage were rather similar, with CoVs of the joint rotation and resistance at the beam-to-column contact state less than 0.05, and those at the ultimate state less than 0.1. The post-ultimate behaviour was variable between different connections, but the CoV of the ductility was only about 0.15. The above data provided important information about the full-range connection behaviour, and the variability in the behaviour due to variable geometrical and material properties, and random imperfections generated during fabrication.

3.2 WA460 tests

Figure 5 shows the test results of specimen WA460-1, including the moment-rotation curve and a selection of pictures illustrating experimental phenomena at different stages. In general, the behaviour of WA460-1 was similar to that of WA360-1 over the full loading range. In the beginning, the connection responded linearly with a large bending stiffness, reaching a resistance of 26.0 kN·m at a rotation of 0.0022 rad. This was followed by

a stage of bolt slip with a jagged plateau in the moment-rotation curve until a rotation of 0.019 rad. At a rotation of 0.105 rad, the beam compression flange came into contact with the column flange, leading to a steep increase in bending stiffness. When the joint rotation reached 0.151 rad, fracture initiated near the root of the angle segment aligning with the top bolt row, and quickly propagated towards the tensile edge of the angle cleat. The ultimate bending resistance was reached soon after, at a moment of 188 kN·m and a corresponding rotation of 0.154 rad, i.e., Point A on the moment-rotation curve in Fig. 5. Subsequently, the crack propagated towards the compressive edge of the angle cleat, leading to the complete failure of the connection. This failure mode was identical to that of the WA360 tests.

Similarly to the WA360 connections, the WA460-1 connection featured changes of bolt bearing states and associated transitions of load-transferring mechanisms. The loading scheme in this test series also generated additional tension in the beam, having a maximum value of 26.7 kN which was reached simultaneously with the ultimate bending resistance. The additional axial tension accounted for only 0.8% of the beam's plastic axial resistance, and hence had a negligible effect compared to the bending moment.

The other WA460 connections behaved similarly to WA460-1, as shown by the moment-rotation curves in Fig. 6. The following variabilities were encountered: *a*) initial stiffness, from 9990 kN·m/rad (WA460-2) to 12000 kN·m/rad (WA460-1); *b*) limit of the initial linear stage, from 9.30 kN·m (WA460-2) to 36.2 kN·m (WA460-3); *c*) rotation at which bolts stopped slipping, from 0.0129 (WA460-4) rad to 0.0188 rad (WA460-1); *d*) resistance when beam-to-column contact occurred, from 97.7 kN·m (WA460-4) to 109 kN·m (WA460-4); *e*) rotation when beam-to-column contact occurred, from 0.105 rad (WA460-1) to 0.127 rad (WA460-2); *f*) ultimate bending resistance, from 176 kN·m (WA460-5) to 190 kN·m (WA460-3); *g*) joint rotation corresponding to the ultimate resistance, from 0.153 rad (WA460-4) to 0.180 (WA460-2); and *h*) joint ductility, determined as the joint rotation when the resistance decreases to 20 kN·m (about 10% of the ultimate strength), from 0.288 rad (WA460-1) to 0.362 rad (WA460-4). Table 3 summarises the results of all WA460 tests. Statistical values of the above joint responses are also presented in the Table. Similarly to the WA360 tests, the resistance of the initial linear stage had the largest variability, while the connection response after the bolt slip stage was relatively less variable.

For all ten connections with two different configurations, the initial linear stage only contributed to a small portion of the total resistance. The connection behaviour subsequent to the initial linear stage was complicated,

246 partly because of the plastic deformation of the load carrying components, notably the web angles, and partly
247 because of the changes of bolt bearing states and the potential for beam-to-column contact. This dynamically
248 changing load-transferring mechanism is not considered in the connection models in [5, 8-12]. To overcome
249 this limitation and thereby predict the full-range behaviour of web angle connections, an advanced component-
250 based mechanical model is proposed in the next section.
251
252 **4. Mechanical model**
253 In this section, the proposed model is first elaborated using web angle connections with three bolt rows,
254 applicable to the WA360 connections. It is subsequently extended to the five-bolt rows connection (WA460
255 specimens). Predictions of the models are validated against the experimental results in Section 5.
256
257 4.1 Static friction and bolt slip stages
258 When a beam is connected to a column using bolted web angles, evidently the clearance of bolt holes
259 prevents load from the beam to be transferred to the column through bearing of bolts, as shown in Fig. 7(a). At
260 this stage, the bending resistance of the connection results from the force couple of the static friction forces at
261 the bolts, and is calculated as:
262 $$M_{sf} = P_f H \tag{4}$$
263 in which H is the distance between the top and bottom bolt rows, and P_f is the static friction force at a bolt, equal
264 to $2\mu F_p$ where F_p is the tensile force in a bolt, and μ is slip factor.
265 For connections using preloaded bolts, the stiffness of the connection during this stage can be obtained
266 through the Component Method in Eurocode 3 Part1-8 [15], in which the stiffnesses of the bolt in shear and the
267 bolt in bearing components are assumed to be infinite (preloaded non-slip condition). For connections using
268 snug tight bolts, the static friction stage is very short because the static friction forces are limited and soon
269 overcome under increasing applied load. In this case, the static friction stage is of relatively little importance in
270 the terms of obtaining the full-range connection behaviour, and it is reasonable to assume a perfectly rigid
271 behaviour for the connection, namely:
272 $$\theta_{sf} = 0 \tag{5}$$

After the static friction forces are overcome, the bolts start to slip until bearing develops against the bolt holes in both the beam web and the angle cleats, as observed in the tests. Kinetic friction forces are almost constant in magnitude during this stage, and therefore, the bending resistance remains largely unchanged, i.e.:

$$M_{bs} = M_{sf} \tag{6}$$

For the experimental program in this study, the column laid horizontally on the supports, and the upright beam was installed to the column. During the installation, the bolts connecting the beam web rested on the bolt holes in the angle cleats due to gravity, and thus the gap between each bolt and the top edge of the bolt hole in the angle cleat was equal to the bolt hole clearance, C, as shown in Fig. 7(a). The bolt holes in the beam web and those in the angle cleats were not always perfectly aligning, generating a gap, denoted by C_b, between the bolt and the bottom edge of the bolt hole in the beam web, as shown in Fig. 7(a). Establishing effective bearing requires the beam rotation to generate travelling distances of C+C_b and C-C_b at the top and bottom bolt holes in the beam web, respectively, as shown in Fig. 7(b). Seeing the angle cleats remain largely undeformed during this stage, the rotation of the connection is all contributed by the rotation of the beam, and is equal to θ_{bs} at the end of the bolt slip stage:

$$\theta_{bs} = \frac{C + C_a + C - C_a}{H} = \frac{2C}{H} \tag{7}$$

The above analysis of connection rotation applies to the experimental specimens tested in this study. On-site assembly creates a different situation with the columns standing upright and the beams being horizontal. In this case, the bolt slip analysis presented in [19] (Fig. 7(c)) showed that the connection rotation at the end of the bolt slip stage can be approximated as:

$$\theta_{bs}^{*} = \frac{2HC}{H^2 - C^2} \tag{7}$$

Normally the clearance is far smaller than the distance between edge bolts, and therefore, the rotation in Eq. (7) can be simplified as:

$$\theta_{bs}^{*} \approx \frac{2HC}{H^2} = \frac{2C}{H} \tag{8}$$

Hence, Eq. (6) holds for on-site installation as well.

297 At the end of the bolt slip stage, the bolt holes in the beam web and in the web angle coincide at the middle
298 bolt row, as shown in Fig. 7(b), leaving a gap of *C* between the bolt and bolt holes. Therefore, the middle bolt
299 does not transfer any load until this gap closes, which requires a greater movement of beam web than the angle
300 cleat at the middle bolt row. This is to be achieved by differential plastic bolt-to-bolt hole bearing deformations
301 at the top and bottom bolt rows, which create a relative rotation between the web angle and the beam, as shown
302 in Fig. 7(d). Note that if the plastic bearing deformation is ideally ignored, the bolt-to-bolt hole gap remains *C*
303 no matter how large the connection rotation, as also depicted in Fig. 7(d). Therefore, the change of bolt bearing
304 states at the middle bolt row cannot be predicted without knowledge of the plastic behaviour of the connection
305 components. The potential beam bottom flange-to-column flange contact relates to the beam rotation, which is
306 also strongly affected by the plastic behaviour of components.
307
308 ## 4.2 Component based mechanical model
309 To accurately predict the behaviour of a web angle connection, it is essential to recognize the change of bolt
310 bearing states at bolt rows, and to distinguish the movement of the web angle from that of the beam end. A
311 model capable of doing so is developed based on the Component Method, as shown in Fig. 8.
312 The model contains three rigid bars, with the support bar representing the column centerline, the middle bar
313 representing the beam leg of web angle (the bar aligns to the centres of the bolt holes in the beam leg), and the
314 side bar representing the beam end (the bar aligns to the centres of the bolt holes in the beam web). It is both
315 necessary and feasible to use an extra rigid bar to model the beam leg of web angle. The necessity stems from
316 the fact that, although at certain bolt rows the bolts on the beam web sometimes are not transferring any load
317 through bearing, the web angle still bends as a whole under the loads transferred through the bolts in bearing,
318 causing loads to be transferred to the column through all tensile bolts connecting the angle cleats to the column
319 flange. The feasibility comes from the fact that, for a web angle, the bending moment from the beam acts in the
320 plane of the beam leg while perpendicular to the column leg, and therefore, the much larger in-plane flexural
321 stiffness enables the beam leg to rotate as a rigid body during the entire loading sequence, as observed in the
322 tests in this study and in other experiments [2-7].
323 The three rigid bars are connected by a series of springs, modelling the components of the connection.
324 Springs between the middle and the side bars model the deformations at the bolt holes in the beam leg of the

web angle and the beam web, and therefore represent the combined deformation of the Bolt in shear component (11) and the Bolt in bearing component (12), as shown in Fig. 8. In web angle connections, tension and compression produce different bolt in bearing behaviours. Under tension, a bolt is bearing towards the edge of the beam web and the edge of the beam leg of the angle, so tear-out failure may occur. Under compression, however, only plastic bearing failure is possible. Hence, the bolt in bearing responses under tension and compression need to be distinguished. For bolt-to-beam web in bearing, the relevant components are Components (12-w, T) and (12-w, C), where T and C represents tension and compression, respectively. For bolt-to-beam leg of angle in bearing, the components are Components (12-a, T) and (12-a, C), as shown in Fig. 8.

All other deformations in the connection occur between the support bar and the middle bar, and are modelled by springs between these two bars, including springs modelling the Column web panel in shear component (1), Column web in transverse compression component (2), Column web in transverse tension component (3), Column flange in bending components (4), Bolt in tension component (10), and Web angle in bending component (21). The Component Method framework in Eurocode 3 Part 1.8 [15] does not include the Web angle in bending component, so in this study a new component index of 21 is temporarily given to this component.

As previously discussed, a connection may have multiple possible states along with the changes of bolt bearing states and contact between column and beam bottom flanges. Figure 9 illustrates all the possible states for a three-bolt row web angle connection. However, generally, all connection states can be modelled by two spring models, i.e., the pre-BCC (beam-to-column contact) model and the post-BCC model, as shown in Fig. 8.

The pre-BCC model contains three spring rows, each representing a bolt row. At a bolt row, springs between neighbouring rigid bars are first assembled in series into two assembled springs, $\mathbf{r}_{i\mathrm{a}}$ between the supporting and the middle bars, and $\mathbf{r}_{i\mathrm{b}}$ between the middle and the side bars, where the subscript i is the bolt row number, as shown in Fig. 8(b). The stiffnesses of Springs $\mathbf{r}_{i\mathrm{a}}$ and $\mathbf{r}_{i\mathrm{b}}$ are $k_{i\mathrm{a}}$ and $k_{i\mathrm{b}}$, respectively.

Under an increment of joint rotation, the incremental deformations of Springs $\mathbf{r}_{i\mathrm{a}}$ and $\mathbf{r}_{i\mathrm{b}}$ are $\Delta d_{i\mathrm{a}}$ and $\Delta d_{i\mathrm{b}}$, respectively. Moment equilibrium and deformation compatibility of the middle bar require:

$$\begin{cases} k_{1\mathrm{a}} \cdot \Delta d_{1\mathrm{a}} \cdot 2w + k_{2\mathrm{a}} \cdot \Delta d_{2\mathrm{a}} \cdot w = k_{1\mathrm{b}} \cdot \Delta d_{1\mathrm{b}} \cdot 2w + k_{2\mathrm{b}} \cdot \Delta d_{2\mathrm{b}} \cdot w \\ \Delta d_{1\mathrm{a}} - \Delta d_{3\mathrm{a}} = 2\left(\Delta d_{2\mathrm{a}} - \Delta d_{3\mathrm{a}}\right) \end{cases} \tag{9}$$

where w is the distance between bolt rows, as shown in Fig. 8(a). Deformation compatibility of the side bar requires:

$$\Delta d_{1b} - \Delta d_{3b} = 2\left(\Delta d_{2b} - \Delta d_{3b}\right) \tag{10}$$

The condition of pure bending requires:

$$\begin{cases} k_{1a} \cdot \Delta d_{1a} + k_{2a} \cdot \Delta d_{2a} + k_{3a} \cdot \Delta d_{3a} = 0 \\ k_{1b} \cdot \Delta d_{1b} + k_{3b} \cdot \Delta d_{3b} + k_{3b} \cdot \Delta d_{3b} = 0 \end{cases} \tag{11}$$

Combining Eqs. (9), (10) and (11), the incremental deformation of all other springs can be related to the incremental deformation of $\mathbf{r}_{1a}$, Δd_{1a}:

$$\begin{cases} \Delta d_{2a} = \dfrac{k_{3a} - k_{1a}}{\alpha_1} \Delta d_{1a} \\ \Delta d_{3a} = -\dfrac{2k_{1a} + k_{2a}}{\alpha_1} \Delta d_{1a} \\ \Delta d_{1b} = \dfrac{\left(k_{2b} + 2k_{3b}\right)\alpha_2}{\alpha_1 \alpha_3} \Delta d_{1a} \\ \Delta d_{2b} = \dfrac{\left(k_{3b} - k_{1b}\right)\alpha_2}{\alpha_1 \alpha_3} \Delta d_{1a} \\ \Delta d_{3b} = -\dfrac{\left(2k_{1b} + k_{2b}\right)\alpha_2}{\alpha_1 \alpha_3} \Delta d_{1a} \end{cases} \tag{12}$$

where $\alpha_1 = k_{2a} + 2k_{3a}$, $\alpha_2 = k_{1a}k_{2a} + 4k_{1a}k_{3a} + k_{2a}k_{3a}$, $\alpha_3 = k_{1b}k_{2b} + 4k_{1b}k_{3b} + k_{2b}k_{3b}$,

Hence, the Pre-BCC rotational stiffness of the connection can be calculated as:

$$K = \frac{\Delta M}{\Delta \theta} = \frac{2w \cdot k_{1b}\Delta d_{1b} + w \cdot k_{2b}\Delta d_{2b}}{\left[\Delta d_{1a} + \Delta d_{1b} - \left(\Delta d_{3a} + \Delta d_{3b}\right)\right] / 2w} = \frac{2w^2 \alpha_2 \cdot \left(k_{1b}k_{2b} + k_{2b}k_{3b} + 4k_{1b}k_{3b}\right)}{\alpha_1\alpha_3 + \left(2k_{1a} + k_{2a}\right)\alpha_3 + \left(2k_{1b} + k_{2b}\right)\alpha_2 + \left(k_{2b} + 2k_{3b}\right)\alpha_2} \tag{13}$$

Under large joint rotation, the beam bottom flange comes into contact with the column flange, beyond which the joint behaviour is modeled by the Post-BCC model. As shown in Fig. 8(c), new compressive springs are introduced aligning with the beam bottom flange to model the compressive deformation at the contact point, and are assembled in series into the assembled spring $\mathbf{r}_4$. The stiffness and incremental deformation of $\mathbf{r}_4$ are k_4 and Δd_4, respectively. Moment equilibrium and deformation compatibility of the middle rigid bar require:

$$\begin{cases} k_{1a} \cdot \Delta d_{1a} \cdot 2w + k_{2a} \cdot \Delta d_{2a} \cdot w = k_{1b} \cdot \Delta d_{1b} \cdot 2w + k_{2b} \cdot \Delta d_{2b} \cdot w \\ \Delta d_{1a} - \Delta d_{3a} = 2\left(\Delta d_{2a} - \Delta d_{3a}\right) \end{cases} \tag{14}$$

Deformation compatibility of the side rigid bar springs requires:

$$\frac{\Delta d_{1a}+\Delta d_{1b}-\Delta d_4}{H_1}=\frac{\Delta d_{2a}+\Delta d_{2b}-\Delta d_4}{H_2}=\frac{\Delta d_{3a}+\Delta d_{3b}-\Delta d_4}{H_3} \tag{15}$$

where H_1, H_2 and H_3 are the distances from the top, middle and bottom bolt rows to the beam bottom flange, respectively, as Shown in Fig. 8(a).

The condition of pure bending requires:

$$\begin{cases} k_{1a}\cdot\Delta d_{1a}+k_{2a}\cdot\Delta d_{2a}+k_{3a}\cdot\Delta d_{3a}+k_4\cdot\Delta d_4=0 \\ k_{1b}\cdot\Delta d_{1b}+k_{2b}\cdot\Delta d_{2b}+k_{3b}\cdot\Delta d_{3b}+k_4\cdot\Delta d_4=0 \end{cases} \tag{16}$$

Combining Eqs. (14), (15) and (16), the incremental deformation of all other springs can be related to the incremental deformation of $\mathbf{r}_{1a}$, Δd_{1a}:

$$\begin{cases} \Delta d_{2a}=\dfrac{-K_{13a}K_b+k_4\left(K_3K_{12b}+K_1K_{23b}\right)}{\beta_1}\Delta d_{1a} \\ \Delta d_{3a}=\dfrac{-K_{12a}K_b+k_4\left(2K_1K_{23b}-K_2K_{13b}\right)}{\beta_1}\Delta d_{1a} \\ \Delta d_4=-\dfrac{\left(K_{13b}+K_{23b}\right)K_a+k_{1b}K_{23a}K_{23b}+k_{2b}K_{13a}K_{13b}+k_{3b}K_{12a}K_{12b}}{\beta_1}\Delta d_{1a} \\ \Delta d_{1b}=\dfrac{\left[\left(h_1-h_2\right)k_{2b}+\left(h_1-1\right)k_{3b}\right]K_a+h_{12}k_{2b}k_{3b}K_{123a}+k_4\beta_2}{\beta_1}\Delta d_{1a} \\ \Delta d_{2b}=\dfrac{\left[-\left(h_1-h_2\right)k_{1b}+\left(h_2-1\right)k_{3b}\right]K_a-2h_{12}k_{1b}k_{3b}K_{123a}+k_4\beta_3}{\beta_1}\Delta d_{1a} \\ \Delta d_{3b}=\dfrac{-\left[\left(h_1-1\right)k_{1b}+\left(h_2-1\right)k_{2b}\right]K_a+h_{12}k_{1b}k_{2b}K_{123a}+k_4\beta_4}{\beta_1}\Delta d_{1a} \end{cases} \tag{17}$$

where $\beta_1=K_{23a}K_b+k_4\left(2K_3K_{12b}+K_2K_{13b}\right)$,

$\beta_2=h_1K_a+h_{12}k_{2b}k_{3b}+k_{2b}\left(h_1k_{1a}-2h_2k_{3a}+h_1k_{3a}\right)+k_{3b}\left(4h_1k_{1a}+k_{2a}+h_1k_{2a}\right)$,

$\beta_3=h_2K_a-2h_{12}k_{1b}k_{3b}+k_{1b}\left(h_2k_{2a}+4h_2k_{3a}-2h_1k_{3a}\right)+4k_{3b}\left(h_2k_{1a}-2k_{1a}+h_2k_{2a}\right)$,

$\beta_4=K_a+h_{12}k_{1b}k_{2b}+k_{1b}\left(k_{2a}+h_1k_{2a}+4k_{3a}\right)+k_{2b}\left(k_{1a}-2h_2k_{1a}+k_{3a}\right)$,

$h_1=H_1/H_3$, $h_2=H_2/H_3$, $h_{12}=1+h_1-2h_2$,

$K_1=k_{1a}+k_{1b}$, $K_2=k_{2a}+k_{2b}$, $K_3=k_{3a}+k_{3b}$, $K_{123a}=k_{1a}+k_{2a}+k_{3a}$, $K_{123b}=k_{1b}+k_{2b}+k_{3b}$,

$K_{12a}=2k_{1a}+k_{2a}$, $K_{13a}=k_{1a}-k_{3a}$, $K_{23a}=k_{2a}+2k_{3a}$,

$K_{12b}=2h_1k_{1b}+h_2k_{2b}$, $K_{13b}=h_1k_{1b}-k_{3b}$, $K_{23b}=h_2k_{2b}+2k_{3b}$,

$$K_a = k_{1a}k_{2a} + k_{2a}k_{3a} + 4k_{1a}k_{3a}\,,\; K_b = 2(h_1 - 1)k_{1b}k_{3b} + (h_2 - 1)k_{2b}k_{3b} + (h_1 - h_2)k_{1b}k_{2b}\,.$$

Hence, the Post-BCC rotational stiffness of the connection can be calculated as:

$$K = \frac{\Delta M}{\Delta\theta} = \frac{H_1 \cdot k_{1b}\Delta d_{1b} + H_2 \cdot k_{2b}\Delta d_{2b} + H_3 \cdot k_{3b}\Delta d_{3b}}{(\Delta d_{1a} + \Delta d_{1b} - \Delta d_4)/H_1}$$
$$= \frac{K_a\left[(h_1 - h_2)^2 k_{1b}k_{2b} + (h_1 - 1)^2 k_{1b}k_{3b} + (h_2 - 1)^2 k_{2b}k_{3b}\right] + K_{123a}k_{1b}k_{2b}k_{3b}h_{12}{}^2 + k_4(h_1k_{1b}\beta_2 + h_2k_{2b}\beta_3 + k_{3b}\beta_4)}{(\beta_1 + h_1K_aK_{123b} + h_{12}k_{2b}k_{3b}K_{123a} + k_{1b}K_{23a}K_{23b} + k_{2b}K_{13a}K_{13b} + k_{3b}K_{12a}K_{12b} + k_4\beta_2)/H_1H_3} \quad (18)$$

4.3 Decision tree for web angle connection model

Figure 9 presents a decision tree, showing possible states of a connection and the conditions leading to these states. In using the decision tree, it needs to be borne in mind is that the connection can fail at any state as long as, in this state, a component fails by reaching its ultimate state. Many connections will not reach the final state, i.e. State (g). For instance, a web angle connection with a very large gap between beam end and column flange is unlikely to bridge the gap and develop contact between the beam compression flange and the column flange, in which case the connection will only reach the State (d) and will fail in this state.

To consider all possible states, as illustrated in Fig. 9, a web angle connection with three bolt rows may experience a total of seven states. Note that in each of the states, yielding of components may occur whereby the stiffness changes. Yielding is tracked in the analysis as the extension of each spring changes under increasing applied rotation. However, the stiffnesses at all states can be calculated through Eqs. (13) and (18) irrespective of whether components respond elastically or inelastically. States prior to beam-to-column contact, i.e. States (a) and (d), employ Eq. (13) developed for the Pre-BCC model, while all the other states employ Eq. (18) developed for the Post-BCC model. When using the equations, springs that are not activated have zero stiffness. Attention should be paid to the stiffness of the bottom bolt row $\mathbf{r}_3$, where compression-to-tension transition may occur, either through States (b), (c), (f) to (g), or through States (e), (f) to (g).

A web angle connection with 3 bolt rows has four criteria leading to transitions between the seven states. The first criterion, Criterion ① in Fig. 9, determines when the bolt at the middle bolt row starts to transfer load from the beam to the column through bearing. As previously discussed and shown in Fig. 7(c), the middle bolt initially does not transfer any load and will continue this non-bearing state (i.e., k_{2b}=0) until the travelling

distance of the bolt hole in the beam web exceeds that of the bolt hole in the web leg of the angle by the bolt hole clearance, C. Therefore, this criterion is that Spring $\mathbf{r}_{2b}$ is activated when and only when the relative displacement between the side and the middle rigid bars is equal to C at $\mathbf{r}_{2b}$.

The second criterion, Criterion ② in Fig. 9, determines when the beam bottom flange comes into contact with the column flange. Evaluating the criterion amounts to calculating when the side rigid bar has a displacement of G (the initial gap between the beam end and the column flange) towards the column flange at spring row $\mathbf{r}_4$. This component-based mechanical model is established with the end of the bolt slip stage being the initial state, and therefore, the initial displacement at Spring $\mathbf{r}_4$ due to connection rotation during the bolt slip stage must be taken into account to achieve an accurate prediction.

The third criterion, Criterion ③ in Fig. 9, determines when compressive force stops to transfer through the bottom bolt row $\mathbf{r}_3$ after beam-to-column contact is established, and thus is only needed after Criterion ②. Establishing of beam-to-column contact at spring row $\mathbf{r}_4$ causes the compressive force at $\mathbf{r}_{3b}$ to unload. When fully unloaded, the bearing state between the bolt and bolt holes at $\mathbf{r}_{3b}$ ceases and Spring $\mathbf{r}_{3b}$ is inactivated. Therefore, this criterion is that Spring $\mathbf{r}_{3b}$ is inactivated when the compressive force in $\mathbf{r}_{3b}$ decreases to zero. Spring $\mathbf{r}_{3a}$ is unloaded along with $\mathbf{r}_{3b}$, and its stiffness changes from compressive stiffness to tensile stiffness, which are very different, after full unloading.

The last criterion, Criterion ④ in Fig. 9, determines when the bolt bearing state is re-established at $\mathbf{r}_{3b}$ under tensile load from the beam web, and is only to be checked after Criterion ③ is satisfied. With a bolt hole clearance of C, re-establishing the bolt bearing state requires the beam web to travel the distance of $2C$ relative to the beam leg of the angle at $\mathbf{r}_{3b}$. Therefore, this criterion is that Spring $\mathbf{r}_{3b}$ is re-activated under tension when and only when the relative displacement between the side and middle rigid bars reaches 2C at the third bolt row.

The above criteria control the path of connection states through the decision tree. The checking of criteria and choosing which path to follow can be easily realised in any programming language, such as Matlab [20].

4.4 Component based mechanical model for connections with five bolt rows

Similar spring models to that shown in Fig. 8 can be developed for web angle connections with different numbers of bolt rows. Herein a model is developed for five-bolt rows connections to predict the behaviour of WA460 specimens. Increasing the number of bolt rows complicates the possible states that a connection may experience. However, generally, all connection states can be modelled by the four spring models shown in Fig. 10.

The bending moment from the beam is first transferred through tension of bolt row $\mathbf{r}_1$ and compression of bolt row $\mathbf{r}_5$. Since the stiffness of tensile springs is usually smaller than that of compressive springs, the centre of rotation of the connection can be either between bolt rows $\mathbf{r_3}$ and $\mathbf{r}_4$, or between bolt rows $\mathbf{r_4}$ and $\mathbf{r}_5$, depending on the stiffnesses of the activated springs. Bolt row $\mathbf{r}_4$ transfers compression in the former case, and tension in the latter case.

With $\mathbf{r}_4$ subjected to tension, the centre of compression of the middle rigid bar is at bolt row $\mathbf{r}_5$, as shown in Fig. 10(b). Therefore, similar to Eqs. (9) and (10), moment equilibrium and deformation compatibility of the middle rigid bar are written as:

$$\begin{cases} 4k_{1a}\Delta d_{1a}+3k_{2a}\Delta d_{2a}+2k_{3a}\Delta d_{3a}+k_{4a}\Delta d_{4a}=4k_{1b}\Delta d_{1b}+3k_{2b}\Delta d_{2b}+2k_{3b}\Delta d_{3b}+k_{4b}\Delta d_{4b} \\ \dfrac{\Delta d_{1a}-\Delta d_{5a}}{4}=\dfrac{\Delta d_{2a}-\Delta d_{5a}}{3}=\dfrac{\Delta d_{3a}-\Delta d_{5a}}{2}=\Delta d_{4a}-\Delta d_{5a} \end{cases} \tag{19}$$

and deformation compatibility of the side rigid bar requires:

$$\frac{\Delta d_{1b}-\Delta d_{5b}}{4}=\frac{\Delta d_{2b}-\Delta d_{5b}}{3}=\frac{\Delta d_{3b}-\Delta d_{5b}}{2}=\Delta d_{4b}-\Delta d_{5b} \tag{20}$$

However, if both $\mathbf{r}_4$ and $\mathbf{r}_5$ are subjected to compression, $\mathbf{r}_4$ becomes the centre of compression for bolt rows above, and the web angle is bent at $\mathbf{r}_4$ under the tensile loads transferred above $\mathbf{r}_4$. In this case, the middle rigid bar above $\mathbf{r}_4$ remains rigid, and the compressive force in $\mathbf{r}_{5b}$ is transferred directly through $\mathbf{r}_{5a}$, as shown in Fig. 10(c). Moment equilibrium and deformation compatibility of the middle rigid bar are re-written as:

$$\begin{cases} 3k_{1a}\Delta d_{1a}+2k_{2a}\Delta d_{2a}+k_{3a}\Delta d_{3a}=3k_{1b}\Delta d_{1b}+2k_{2b}\Delta d_{2b}+k_{3b}\Delta d_{3b} \\ k_{5a}\Delta d_{5a}=k_{5b}\Delta d_{5b} \\ \dfrac{\Delta d_{1a}-\Delta d_{4a}}{3}=\dfrac{\Delta d_{2a}-\Delta d_{4a}}{2}=\Delta d_{3a}-\Delta d_{4a} \end{cases} \tag{21}$$

and deformation compatibility of the side rigid bar becomes:

$$\frac{\Delta d_{1a}+\Delta d_{1b}-\left(\Delta d_{5a}+\Delta d_{5b}\right)}{4}=\frac{\Delta d_{2a}+\Delta d_{2b}-\left(\Delta d_{5a}+\Delta d_{5b}\right)}{3}=\frac{\Delta d_{3a}+\Delta d_{3b}-\left(\Delta d_{5a}+\Delta d_{5b}\right)}{2}$$
$$=\Delta d_{4a}+\Delta d_{4b}-\left(\Delta d_{5a}+\Delta d_{5b}\right) \tag{22}$$

The condition of pure bending is the same for both cases:

$$\begin{cases} k_{1a}\Delta d_{1a}+k_{2a}\Delta d_{2a}+k_{3a}\Delta d_{3a}+k_{4a}\Delta d_{4a}+k_{5a}\Delta d_{5a}=0 \\ k_{1b}\Delta d_{1b}+k_{2b}\Delta d_{2b}+k_{3b}\Delta d_{3b}+k_{4b}\Delta d_{4b}+k_{5b}\Delta d_{5b}=0 \end{cases} \tag{23}$$

Hence, different loading conditions at the $\mathbf{r}_4$ bolt row lead to different pre-BCC models. The model shown in Fig. 10(b) is referred to as the Pre-BCC-$\mathbf{r}_4$T model to describe the tensile loading state of $\mathbf{r}_4$, and is characterised by Eqs. (19), (20) and (23), while the model shown in Fig. 10(c) is referred to as the Pre-BCC-$\mathbf{r}_4$C model with $\mathbf{r}_4$ receiving compression, and is characterised by Eqs. (21), (22) and (23). The connection stiffnesses from the pre-BCC models are calculated using:

$$K=\frac{\Delta M}{\Delta\theta}=\frac{w^2\left(4k_{1b}\dfrac{\Delta d_{1b}}{\Delta d_{1a}}+3k_{2b}\dfrac{\Delta d_{2b}}{\Delta d_{1a}}+2k_{3b}\dfrac{\Delta d_{3b}}{\Delta d_{1a}}+k_{4b}\dfrac{\Delta d_{4b}}{\Delta d_{1a}}\right)}{1+\dfrac{\Delta d_{1b}}{\Delta d_{1a}}-\left(\dfrac{\Delta d_{2a}}{\Delta d_{1a}}+\dfrac{\Delta d_{2b}}{\Delta d_{1a}}\right)} \tag{24}$$

in which the items $\Delta d_{1b}/\Delta d_{1a}$, $\Delta d_{2b}/\Delta d_{1a}$, $\Delta d_{3b}/\Delta d_{1a}$, $\Delta d_{4b}/\Delta d_{1a}$ and $\Delta d_{2a}/\Delta d_{1a}$ are solved through Eqs. (19), (20) and (23), or through Eqs. (21), (22) and (23), depending on which model is used. This method is the same as that used in the three-bolt rows mechanical models. But the solution of the equations is more complex than those presented in Eqs. (12) and (17), so the expression for the connection stiffness is not presented in this paper. However, the linear nature of the equations enables them to be easily solved by mathematical manipulation software, such as the symbolic-computing toolbox MuPAD embedded in Matlab [20]. This is how the above equations are solved in this study for the five-bolt rows mechanical model.

After the beam bottom flange comes into contact with the column flange, the connection behaviour can be described by two post-BCC models, as shown in Fig. 10(d) and 10(e), depending on the loading condition of the $\mathbf{r}_4$ bolt row. The Post-BCC-$\mathbf{r}_4$T model is used for connection states with $\mathbf{r}_4$ bolt row under tension, and is characterised by Eqs. (19), (25) and (26), while the Post-BCC-$\mathbf{r}_4$C model is used in the case of $\mathbf{r}_4$ bolt row under compression, and is characterised by Eqs. (21), (25) and (26).

$$\frac{\Delta d_{1a}+\Delta d_{1b}-\Delta d_6}{h_1}=\frac{\Delta d_{2a}+\Delta d_{2b}-\Delta d_6}{h_2}=\frac{\Delta d_{3a}+\Delta d_{3b}-\Delta d_6}{h_3}=\frac{\Delta d_{4a}+\Delta d_{4b}-\Delta d_6}{h_4}=\frac{\Delta d_{5a}+\Delta d_{5b}-\Delta d_6}{h_5} \tag{25}$$

$$\begin{cases} k_{1a}\cdot\Delta d_{1a}+k_{2a}\cdot\Delta d_{2a}+k_{3a}\cdot\Delta d_{3a}+k_{4a}\cdot\Delta d_{4a}+k_{5a}\cdot\Delta d_{5a}+k_{6}\cdot\Delta d_{6}=0 \\ k_{1b}\cdot\Delta d_{1b}+k_{2b}\cdot\Delta d_{2b}+k_{3b}\cdot\Delta d_{3b}+k_{4b}\cdot\Delta d_{4b}+k_{5b}\cdot\Delta d_{5b}+k_{6}\cdot\Delta d_{6}=0 \end{cases} \tag{26}$$

The connection stiffnesses from the post-BCC models are calculated using:

$$K=\frac{\Delta M}{\Delta\theta}=\frac{H_1\left(H_1k_{1b}\dfrac{\Delta d_{1b}}{\Delta d_{1a}}+H_2k_{2b}\dfrac{\Delta d_{2b}}{\Delta d_{1a}}+H_3k_{3b}\dfrac{\Delta d_{3b}}{\Delta d_{1a}}+H_4k_{4b}\dfrac{\Delta d_{4b}}{\Delta d_{1a}}+H_5k_{5b}\dfrac{\Delta d_{5b}}{\Delta d_{1a}}\right)}{1+\dfrac{\Delta d_{1b}}{\Delta d_{1a}}-\dfrac{\Delta d_{6}}{\Delta d_{1a}}} \tag{27}$$

in which the items $\Delta d_{1b}/\Delta d_{1a}$, $\Delta d_{2b}/\Delta d_{1a}$, $\Delta d_{3b}/\Delta d_{1a}$, $\Delta d_{4b}/\Delta d_{1a}$, $\Delta d_{5b}/\Delta d_{1a}$ and $\Delta d_{6}/\Delta d_{1a}$ are solved through Eqs. (19), (24) and (25), or through Eqs. (21), (24) and (25), depending on which of the post-BCC models is used. Similarly, the equations can be solved through symbolic-computing software such as MuPAD in Matlab [20].

It is noted that the initial state of bolt row $\mathbf{r}_4$ in post-BCC loading is inherited from the last pre-BCC loading state. Consequently, if the last loading state of bolt row $\mathbf{r}_4$ in the pre-BCC stage is tension, bolt row $\mathbf{r}_4$ will keep the current tensile loading state in the post-BCC stage, and will not change to the compressive loading state as long as the connection is under monotonic bending. On the other hand, if bolt row $\mathbf{r}_4$ is under compression in the pre-BCC stage, the compressive force in bolt row $\mathbf{r}_4$ will unload in post-BCC stage until the compressive force is fully unloaded, as described by the Post-BCC-$\mathbf{r}_4$C model.

A web angle connection with five bolt rows has a large number of possibilities for the bearing state of each bolt, both prior to and after beam-to-column contact, making the decision tree of the mechanical model considerably more complex than the one shown in Fig. 8. Hence, this paper does not provide the complete decision tree. Instead, the fundamental criteria, similar to those previously described for the three-bolt rows mechanical model in Section 4.3, are introduced to guarantee the accurate path in the decision tree is followed when employing the mechanical model:

(1) The beam bottom flange comes into contact with the column flange when the side rigid bar has a displacement of G towards the column flange at $\mathbf{r}_6$;

(2) Spring $\mathbf{r}_{2b}$ is activated in tension when the relative displacement between the side and the middle rigid bars reaches $0.5C$ at $\mathbf{r}_{2b}$;

(3) Spring $\mathbf{r}_{3b}$ is activated in tension when the relative displacement between the side and the middle rigid bars reaches C at $\mathbf{r}_{3b}$;

(4) Prior to BCC, Spring $\mathbf{r}_{4b}$ is activated in tension when the relative displacement between the side and the middle rigid bars reaches $1.5C$ at $\mathbf{r}_{4b}$, and is activated in compression when the relative displacement is equal to $-0.5C$;

(5) A compressive bearing spring ($\mathbf{r}_{5b}$, and possibly $\mathbf{r}_{4b}$) unloads as soon as BCC occurs, and is inactivated when the compressive force in the spring has decreased to zero;

(6) Spring $\mathbf{r}_{5b}$ is re-activated in tension when the relative displacement between the side and middle rigid bars reaches $2C$ at $\mathbf{r}_{5b}$ in the post-BCC stage;

(7) The connection fails as soon as any of the component fails by reaching its ultimate strength.

With the above criteria implemented, the mechanical model is applied to predicting the behaviour of the WA460 specimens tested in this study. Figure 11 shows the path that the connection follows through the decision tree. More details about the prediction results are presented in Section 5.

4.5 Post-ultimate behaviour

The outermost spring rows transfer the largest load, and are normally where failure of components starts. The failure of an outermost spring row, either on the tensile side or on the compressive side, implies a redistribution of loads transferred by other spring rows. If the connection were to continue to transfer the moment applied at failure of the outermost spring row, the load to be transferred by remaining bolt rows would exceed their capacity, leading to a progressive failure. Therefore, the failure of a component marks the ultimate bending strength of the connection. However, increasingly, the post-ultimate behaviour is also of interest; for example, in design by advanced (GMNIA) analysis, in which members and connections may be loaded past their ultimate strength.

An energy-based approach, similar to that proposed in [21], is adopted herein to approximately determine the post-ultimate behaviour. After a component fails, the connection loses the bending resistance provided by failed component, $M_{\text{f\_spr}}$. Thus, the residual bending resistance after the component failure, M_{res}, is:

$$M_{\text{res}} = M_{\text{pre}} - M_{\text{f\_spr}} \tag{28}$$

where M_{pre} is the connection bending resistance prior to component failure.

The failure of the component immediately releases all the potential energy stored in the spring row, E_{f_spr}, which implies that the connection develops further rotation. As the propagation of fracture in the web angle is usually unstable and consecutive, it is assumed that failure of the next spring row occurs as soon as this amount of released energy is absorbed during the connection rotation. Therefore, the connection rotation corresponding to the residual bending resistance, M_{res}, is:

$$\theta_{res} = \theta_{pre} + \frac{E_{f\_spr}}{\left(M_{ult} + M_{res}\right)/2} \tag{29}$$

where θ_{pre} is the connection rotation corresponding to M_{pre}.

Failure of spring rows propagates until the last spring row fails, and Eqs. (28) and (29) can be repeated to obtain the entire post-ultimate connection behaviour. The above energy based method ignores the potential of the remaining bolt rows to carry higher load under increasing connection rotation, and thus may be slightly conservative. However, as the failure of web angle connections features a typical progressive fracture mode, the above assumption is found to lead to accurate predictions, as shown in Section 5.

4.6 Web angle in bending component

The deformation of the web angles is a major contributor to the rotation of a web angle connection, and its accurate characterisation is crucial for predicting the full-range behaviour of the connection. A web angle spans multiple bolt rows and deforms continuously. In order to incorporate the continuous deformation of a web angle into the spring rows-based mechanical model, the web angle is discretised into multiple segments, each corresponding to a bolt row, as shown in Fig. 12(a) and implied in Fig. 8(a). Within an angle segment, the deformation of all cross sections is assumed identical, represented by the deformation at the bolt row which is in the middle of the segment. Therefore, the displacements of the middle rigid bar at bolt rows are the characteristic deformation of angle segments, and the continuity of web angle deformation is guaranteed by the deformation compatibility of the middle rigid bar. For double web angle connections, a Web angle in bending component, i.e., Component (21) shown in Fig. 8, comprises a pair of back-to-back web angle segments.

After discretisation, an angle segment has the same deformation pattern as a tensile flange cleat used in top and seat angle connections, as seen from the comparison shown in Fig. 12. Therefore, the behaviour of a Web

angle in bending component can be obtained using models developed for Top flange angle in bending component, which are available in [22].

5. Mechanical model prediction and validation

5.1 Model parameters

Model parameters related to the static fraction and bolt slip stages are first determined, including the tensile force in a bolt, F_p, and slip factor, μ. Connections tested in this study used snug tight bolts, the tensile force in which is not specified by design specifications and varies from application to application. The approximation is made herein that firmly tightening a snug tight bolt generates a tensile force in the bolt of 40% of the design preloading force in a preloaded bolt. Therefore, F_p is equal to 68.6 kN (= 0.4 x 0.7 x 1000MPa x 245mm^2), where the slip factor μ is taken as 0.4 [15].

The properties of components are to be determined for the spring models. The Bolt in bearing component (Component 12) and Web angle in bending component (Component 21) contribute to the major plastic deformation in a web angle connection, and therefore, the plastic properties of these two components have to be taken into account. All other components are assigned with linear elastic properties, with the initial stiffness and resistance obtained from Eurocode 3 Part 1-8 [15].

No reliable mechanical model is available for predicting the full-range response of the Bolt in bearing component. In the absence of such model, a bilinear force-displacement relationship is assumed herein as a practical approximation. For Components (12-w, T) and (12-w, C), the initial stiffness is calculated according to Eurocode 3 Part 1-8 [15], and the elastic limit is adopted as 2/3 of the Eurocode 3 resistance. This is because the resistance given by Eurocode 3 is a strength comprising both the elastic and some of the post-elastic strength, and Eurocode 3 implicitly gives the contributing component of the joint a reduction in stiffness in the last 1/3 of its resistance through an empirical equation, thus accounting for the post-yielding nonlinear behaviour. The post-yielding stiffness is assumed as 5% of the initial stiffness, which is commonly used in other research programs [21, 23-24]. In double web angle connections, Components (12-a, T) and (12-a, C) have relatively large strength as at each bolt row a bolt bears against two angle cleats. For the specimens tested in this study, the elastic limits of Components (12-a, T) and (12-a, C) are higher than the ultimate strength of the component

585 that fails, i.e. the Web angle in bending component (Component 21). Hence, these two components adopt elastic
586 linear force-displacement curve.

587 The behaviour of the Web angle in bending component can be obtained using models for the Top flange
588 angle in bending component, as previously discussed. Eurocode 3 Part 1-8 provides such a model by simplifying
589 a top flange angle into a T-stub [15]. However, recent research [22] showed that the T-stub model in Eurocode
590 3 significantly underestimates the resistance of a top flange angle by more than 85%. A mechanical model is
591 proposed in [22] which shows significantly better accuracy than the Eurocode 3 T-stub model in predicting
592 ultimate strength, and is also capable of accurately predicting the ductility of the component. The model is
593 adopted in this present study but modified to increase the ultimate strength by 50%. This is because it was shown
594 in [22] that the ultimate strength is consistently underestimated by approximately 1/3 because the model ignores
595 the effect of catenary action developing in the angle under large deformation. Moreover, for the sake of
596 simplicity, the original quadri-linear force-displacement curve is simplified into a bi-linear curve, as shown in
597 Fig. 13. The web angles used in the WA360 and WA460 connections had identical profiles and the same bolt
598 spacing, and thus the Web angle in bending components in the two connections are identical. Figure 13 shows
599 the force-displacement curve of the Web angle in bending component, applicable to both connections. Tables 4
600 and 5 summarise the properties of the components in the WA360 and WA460 connections, respectively.
601

602 ## 5.2 Prediction and validation

603 Figure 14 presents the prediction of the proposed mechanical model for the WA360 connection, and its
604 comparison against the experimental results. The model accurately predicts the force-displacement curve, by
605 precisely capturing all the experimental phenomena, including slip of bolts in the initial stage, yielding of
606 components, bearing condition of each bolt, contact between the beam bottom flange and the column flange,
607 occurrence of fracture, and the post-fracture behaviour. The model provides useful information about the
608 distribution of loads within the connection, which is normally not easily obtained from tests. According to the
609 model prediction, in WA360, the bolt at the middle bolt row started bearing slightly prior to the beam-to-column
610 contact, and the bolt at the bottom bolt row began to transfer tensile load before the occurrence of fracture in
611 the web angle. This demonstrates a path of (a)-(d)-(e)-(f)-(g) in the decision tree (Fig. 9) for this connection. A
612 transition of bearing states from under compression to under tension is observed at the bottom bolt. Moreover,

613 the yielding sequence of the components is also distinctly seen from the model prediction between points 3 and
614 13 on the moment-rotation curve.

615 Figure 15 presents the model prediction for the WA460 connection. Good agreement is again observed
616 between the model prediction and the experimental results in terms of moment-rotation response. With two
617 more bolt rows on the beam web, the connection experienced more changes of load transferring mechanisms
618 than the WA360 connection, which are all explicitly captured by the model prediction. Soon after the initial bolt
619 slip stopped, the bolt at the second bolt row from the top started to transfer tensile load, and slightly after that,
620 the bolt at the fourth bolt row from the top began to transfer compressive load. Subsequently, the beam bottom
621 flange came into contact with the column flange, after which bolt bearing in compression at the fourth and
622 bottom bolt rows stopped and bolt bearing in tension at the middle bolt row commenced. The connection failed
623 due to fracture in the web angle at the top bolt row, which was before bolt bearing could be re-established at the
624 fourth and the bottom bolt rows. The above transition of connection states is illustrated in Fig. 11. The model
625 prediction also captures the yielding sequence of the components occurring between points 3 and 17 on the
626 moment-rotation curve.

627 Overall, the proposed model accurately predicts the full-range behaviour of web angle connections. Five
628 comments are made herein on the applicability of the model. Firstly, although the model predicts the failure
629 mode of web angle fracture for both WA360 and WA460, it is capable of predicting all the possible failure
630 modes as long as accurate ultimate strength and ductility models of the corresponding components are provided.
631 Secondly, the model works very well for WA360 and WA460 in the post-ultimate range, in which the
632 connection failure featured progressive fracture in the web angle. For other failure modes such as tear-out at
633 bolt holes, the connection failure is not as progressive as the web angle fracture mode, and the remaining bolt
634 rows can sustain load under increasing connection rotation. In that case, the proposed model is slightly on the
635 conservative side in the post-ultimate range. Thirdly, the model has the potential to be developed into models
636 that apply to more complicated loading conditions. By replacing the pure bending condition, i.e., Eqs. (11), (16),
637 (23) and (26), by an axial force equilibrium condition, the modified model can consider the effect of axial force
638 on the connection. Fourthly, the model can predict hysteresis behaviour of web angle connections as it is capable
639 of tracking the real-time bolt bearing state and the associated loading transferring mechanism. Finally, while
640 other connection models reported in the literature may be unable to analyse connections with both flange and

641 web angles, the proposed model is readily extended to model top-and-seat angle connections with web angles,
642 simply by adding top and seat angle components to the model.
643
644 **6. Conclusion**
645 This paper presents an investigation of the flexural behaviour of double web angle connections. Experiments
646 were carried out on ten specimens to study the connection behaviour from initial linear stage to complete failure
647 involving yielding and fracture. A component-based mechanical model was proposed, providing a useful tool
648 for predicting the full-range connection behaviour.
649 The test program examined two connection configurations, featuring three and five rows of bolts. For both
650 configurations, the connection experienced, in sequence, an initial linear range, a bolt slip stage generating a
651 plateau on the moment-rotation curve, a nonlinear response associated with plastic deformation of angle cleats,
652 contact between beam compressive flange and column flange, steep increase in resistance following contact
653 between beam and column, and connection failure featuring progressive fracture in the angle cleats along the
654 root. The initial linear stage contributed to only a small portion of the total resistance, and the load-transferring
655 mechanism of the connection changed several times due to the changes of bolt bearing states at the middle and
656 bottom bolt rows.
657 For each connection configuration, five identical specimens were tested so as to evaluate the variability in
658 the full-range connection behaviour. Due to highly uncertain tensile forces in the snug tight bolts, the resistance
659 limit of the initial linear stage was highly variable, with a CoV over 0.5. On the contrary, the connection response
660 after the bolt slip stage showed much less variability. The connection resistance and rotation at the point of
661 beam-to-column contact and at the ultimate limit state, had CoVs less than 0.1.
662 Seeing the available models for web angle connections are not capable of capturing the complicated
663 transitions of load-transferring mechanism, a component-based mechanical model was proposed to predict the
664 full-range behaviour of web angle connections. This model uses three rigid bars to respectively represent the
665 column centerline, the beam leg of the web angle, and the beam end. A decision tree is introduced to track the
666 evolution of the load-transferring mechanism of the connection, including the bearing state of each bolt, either
667 under tensile or compressive load, contact state between the beam bottom flange and column flange, plastic
668 deformation of the critical connection components, and the progressive propagation of fracture in the connection.

669 The proposed model was applied to the tested connections in this study and validated against the
670 experimental observations. The predicted full-range force-displacement curves are close to the experimental
671 curves, indicating excellent agreement between the model predictions and the experimental results. Moreover,
672 the model predictions also provide insight into the load distribution within the connection, which is normally
673 not easily obtained from tests.
674
675 **Acknowledgement**
676 The work presented in this paper was funded by the Australian Research Council, via Discovery Project
677 DP150104873.
678
679 **References**
680 [1] Kong, Z. and Kim, S. Numerical estimation of the initial stiffness and ultimate moment capacity of single-
681 web angle connections. J. Constr. Steel Res. 121 (2016) 282–290.
682 [2] Lipson, S.L. Single-angle and single-plate beam framing connections. In: Proceedings of the Canadian
683 Structural Engineering Conference, Toronto, Ontario 1968, 141–162.
684 [3] Altman Jr., W.G., Azizinamini, A., Bradburn, J.H. and Radziminski, J.B. Moment-rotation characteristics
685 of semi-rigid steel beam-column connections. Dept. of Civ. Eng., University of South Carolina, Charleston,
686 S.C., USA, 1982.
687 [4] Astaneh, A., Nader, M.N. and Malik, L. Cyclic behavior of double angle connections. J. Struct. Eng. 115(5)
688 (1989) 1101–1118.
689 [5] Hong, K., Yang, J.G. and Lee, S.K. Moment-rotation behavior of double angle connections subjected to
690 shear load. Eng. Struct. 24(1) (2002) 125–132.
691 [6] Abolmaali A., Kukreti A.R., and Razavi, H. Hysteresis behavior of semi-rigid double web angle steel
692 connections. J. Constr. Steel Res. 59(8) (2003) 1057-1082.
693 [7] Gong, Y.L. Single-angle all-bolted shear connection. J. Constr. Steel Res. 65(6) (2009) 1337–1345.
694 [8] Kishi, N. and Chen, W. F. Moment-Rotation Relations of Semirigid Connections with Angles. J. Struct.
695 Eng. 116(7) (1990) 1813–1834.

696 [9] Lee, S.S. and Moon, T.S. Moment-rotation model of semi-rigid connections with angles. Eng. Struct. 24(2)
697 (2002) 227–237.
698 [10] Yang, J.G. and Lee, G.Y. Analytical models for initial stiffness and ultimate moment of a double angle
699 connection, Eng. Struct. 29(4) (2007) 542–551.
700 [11] Gong, Y.L. Design moment of shear connections at the ultimate limit state. J. Constr. Steel Res. 65(6)
701 (2009) 1921–1930.
702 [12] Kong, Z. and Kim, S. Moment-rotation model of single-web angle connections. Int. J. Mech. Sci. 126 (2017)
703 24–34.
704 [13] Zhu, C., Rasmussen, K.J.R., Yan, S. and Zhang, H. Experimental full-range behaviour assessment of bolted
705 moment end-plate connections, J. Struct. Eng. 145(8) (2019) 04019079.
706 [14] Sakurai, S., Ellingwood, B. R., Kushiyama, S. Probabilistic study of the behaviour of steel frames with
707 partially restrained connections, Eng. Struct. 23 (2001) 1410–1417.
708 [15] CEN (European Committee for Standardization), EN 1993-1-8, Eurocode 3: design of steel structures, Part
709 1-8: design of joints, Eur. Comm. Stand. Brussels, 2010.
710 [16] AS/NZS 1252.1, High-strength steel fastener assemblies for structural engineering – Bolts, nuts and
711 washers, Standards Australia/Standards New Zealand, 2016.
712 [17] ANSI/AISC 360-10. Specification for structural steel buildings. American Institute of Steel Construction;
713 2010.
714 [18] AS/NZS 3679, Hot-Rolled Bars and Sections, Standards Australia/Standards New Zealand, 2010.
715 [19] Yan, S., Rasmussen, K.J.R., Liu, X., Dai, L. and Zhao, X. Behaviour of H-section purlin connections in
716 resisting progressive collapse of roofs. Eng. Struct. 201 (2019) 109849.
717 [20] Matlab ver. R2018b.
718 [21] Zhu, C., Rasmussen, K.J.R. and Yan, S. Generalised component model for structural steel joints. J. Constr.
719 Steel Res. 153 (2019) 330–342.
720 [22] Yan, S., Jiang, L., Rasmussen, K.J.R. and Zhang, H. Full-range behaviour of top and seat angle connections.
721 Submitted to Journal of Structural Engineering.
722 [23] Simões Da Silva, L., Santiago, A., Vila Real, P. Post-limit stiffness and ductility of endplate beam-to-
723 column steel joints, Comput. Struct. 80 (2002) 515–531.

[24] Del Savio, A.A., Nethercot, D.A., Vellasco, P.C.G.S., Andrade, S.A.L., Martha, L.F. Generalised component-based model for beam-to-column connections including axial versus moment interaction, J. Constr. Steel Res. 65 (8) (2009) 1876–1895.

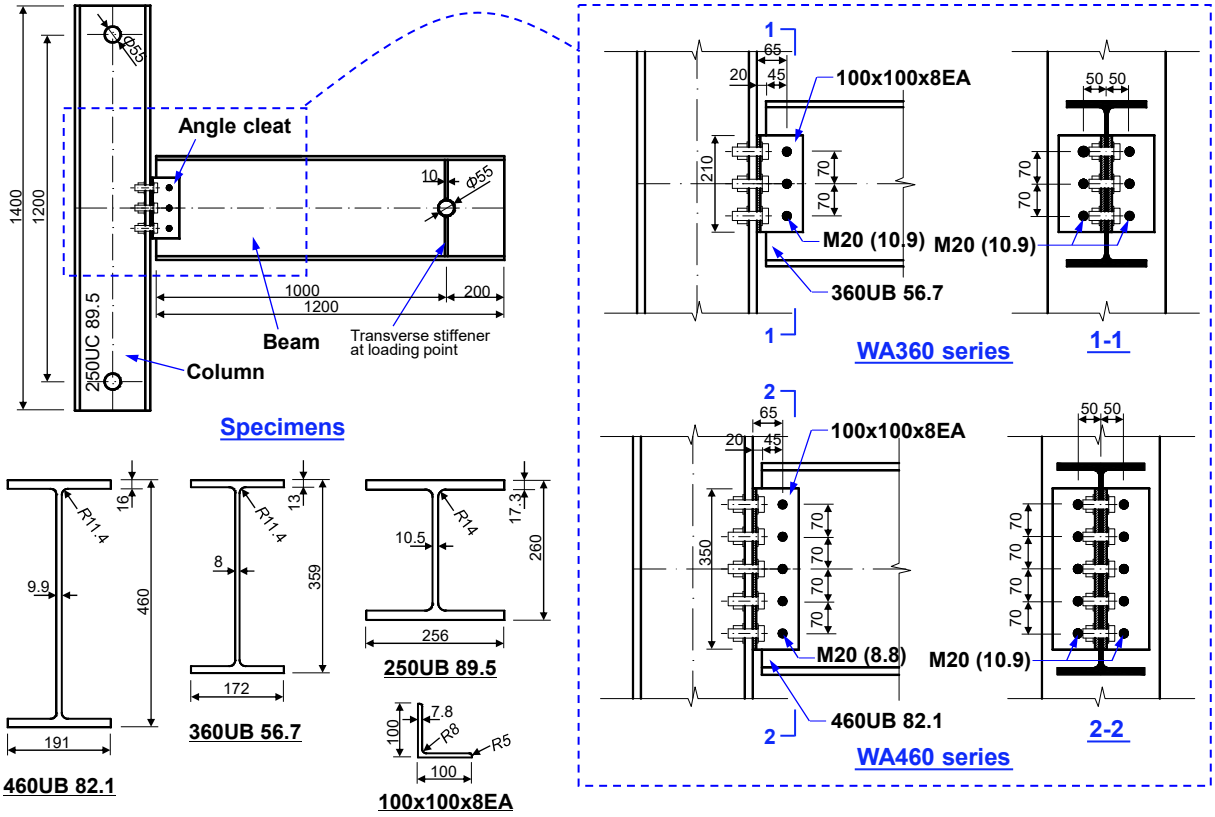

Fig. 1. Geometry of specimens (all dimensions in mm).

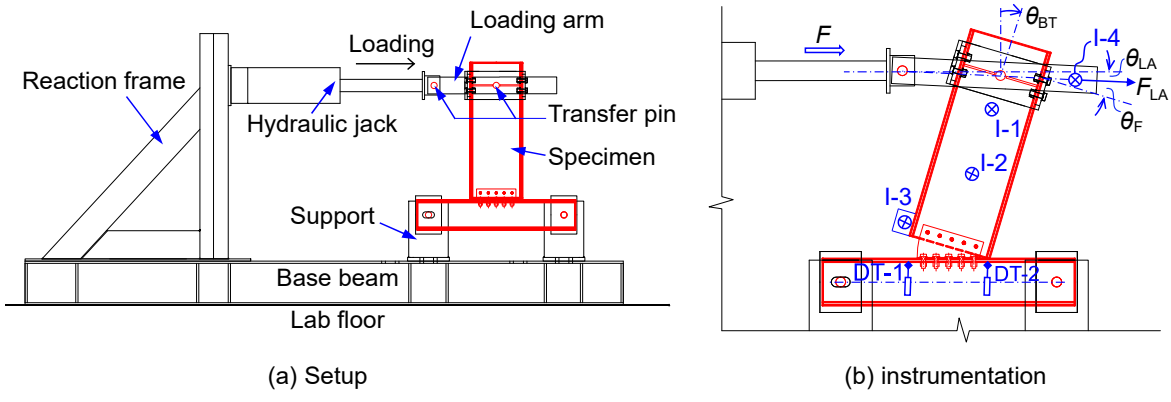

(a) Setup (b) instrumentation

Fig. 2. Test setup and instrumentation.

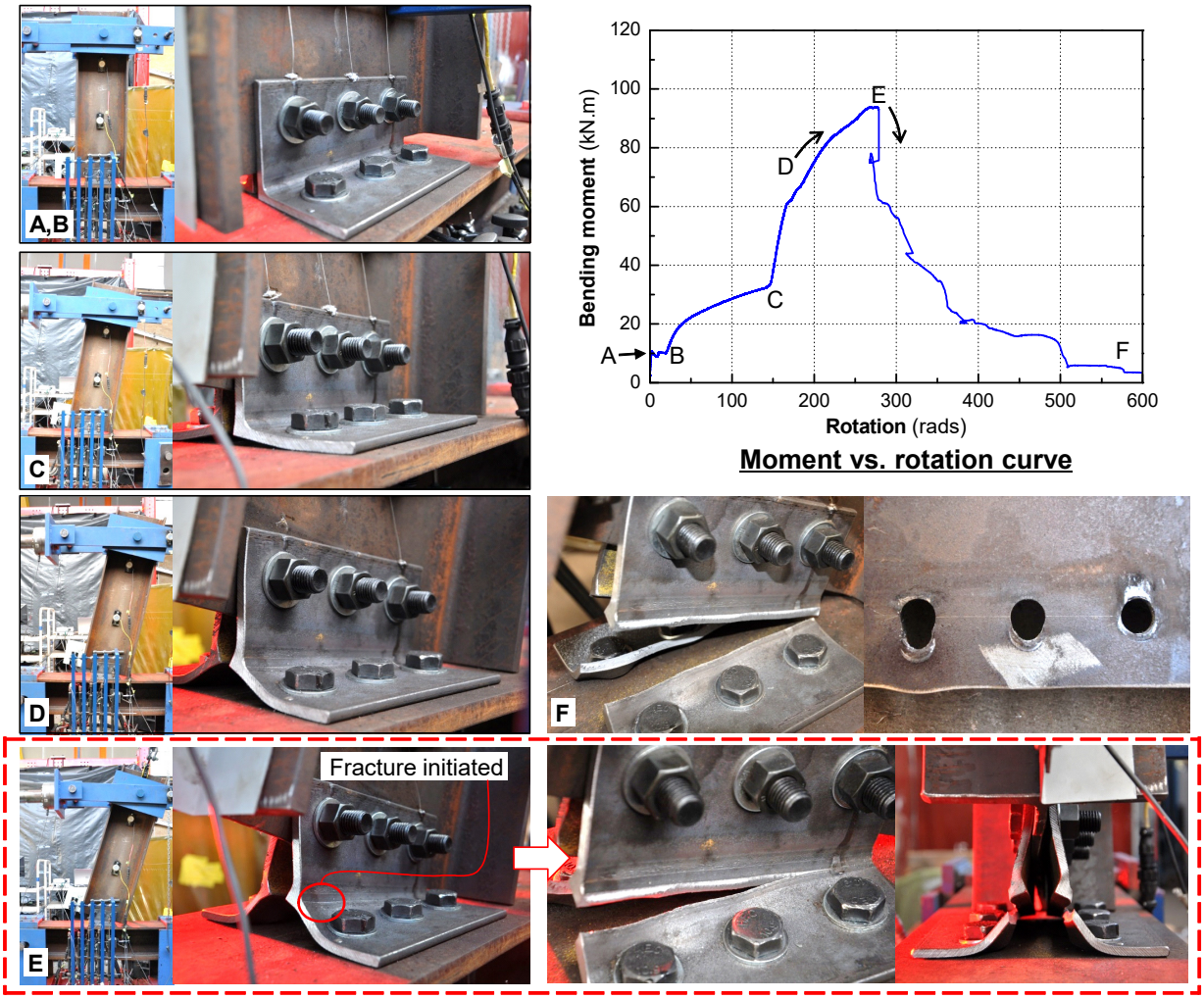

Fig. 3. Test results of WA360-1

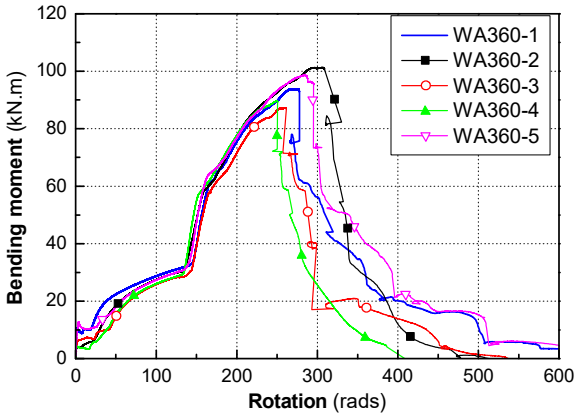

Fig. 4. Moment-rotation curves of the WA360 series tests

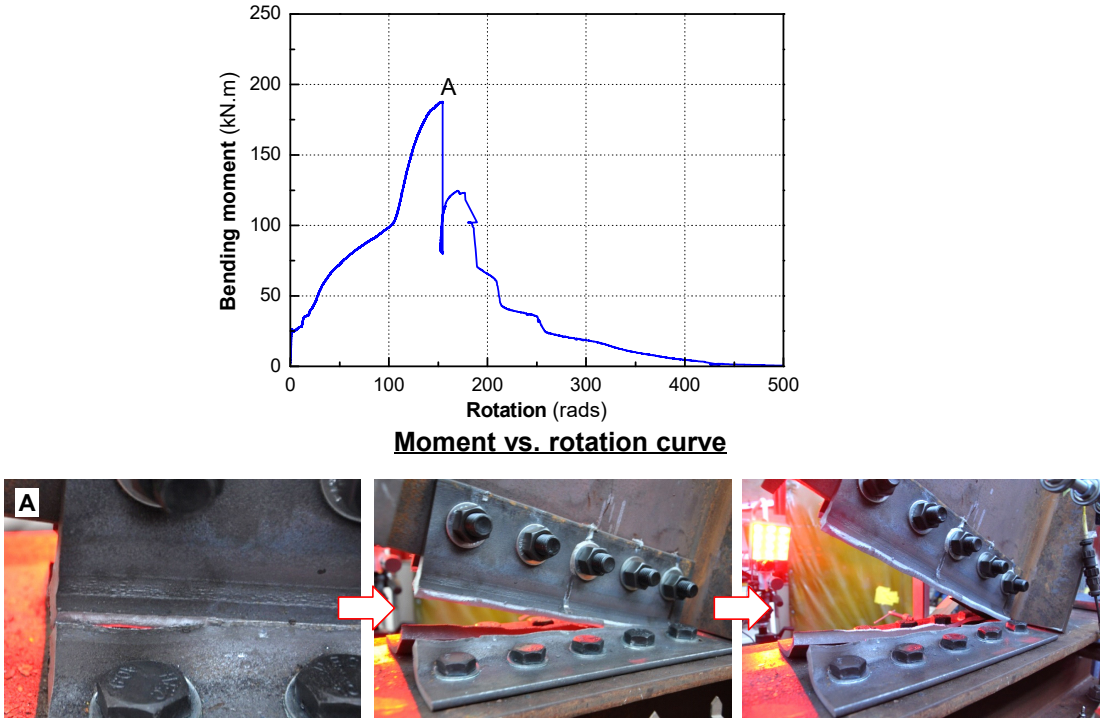

Fig. 5. Test results of WA460-1

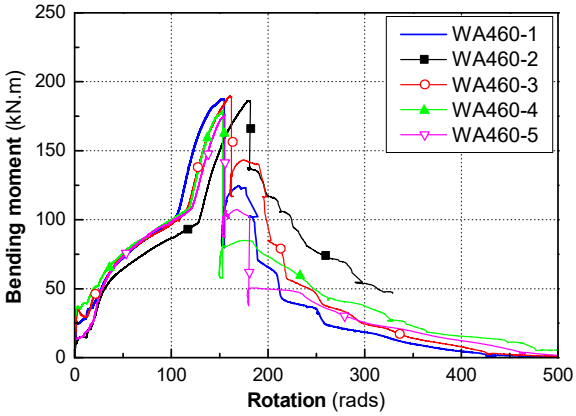

Fig. 6. Test results of WA460 series

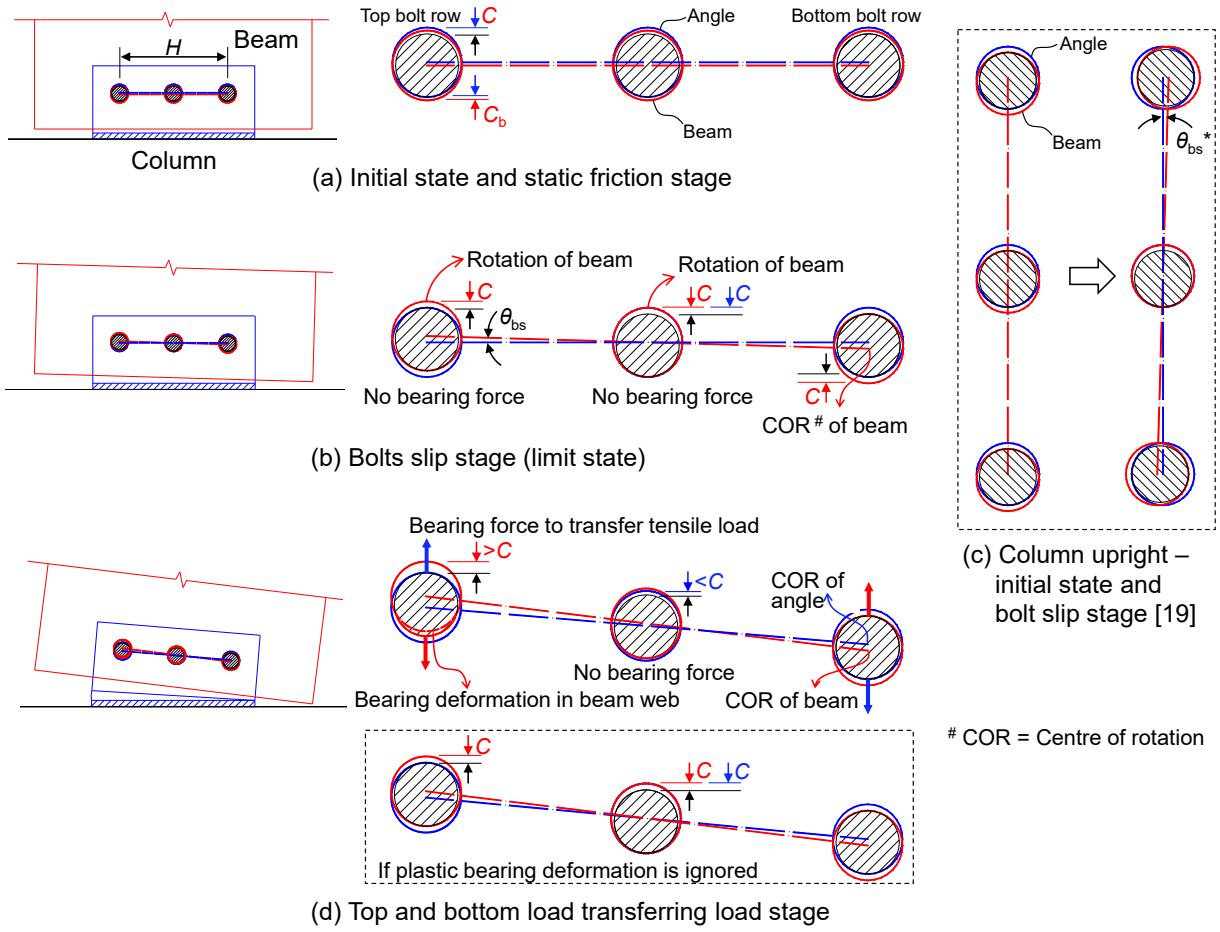

Fig. 7. Deformation pattern and load transferring mechanisms prior to beam-to-column contact.

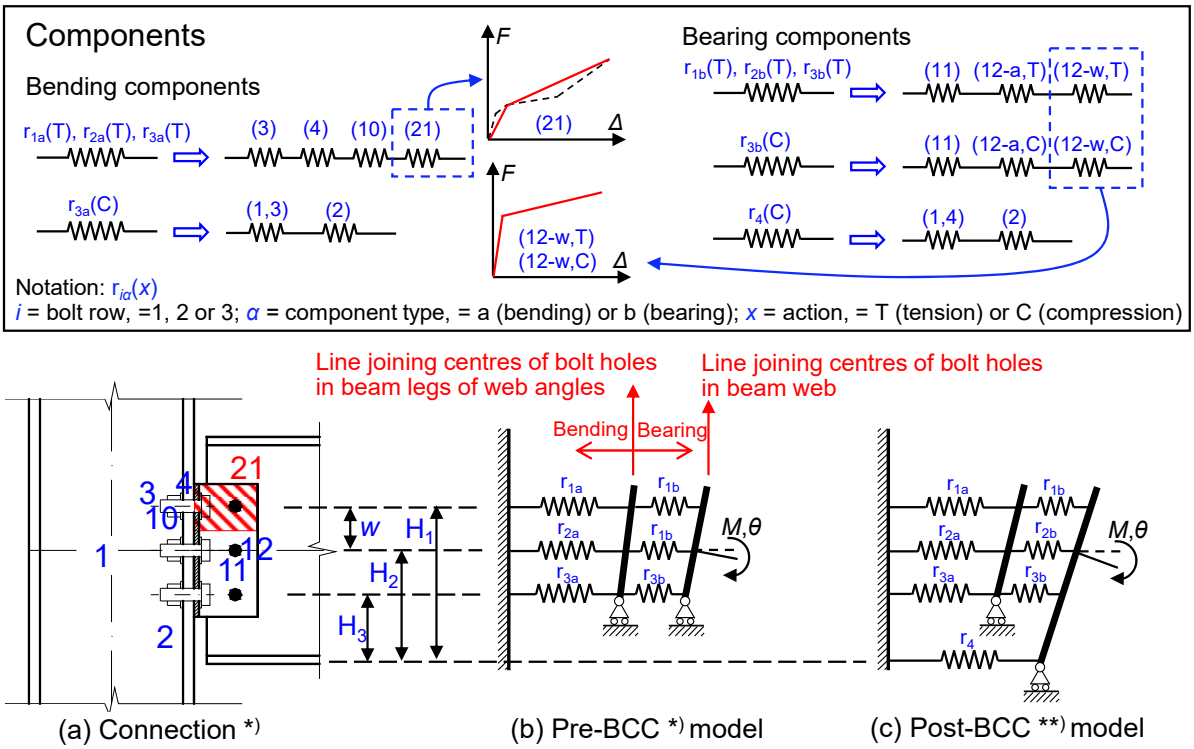

*) The numbers define the component numbers in accordance with Eurocode3 Part 1.8, except for component No. 21 which is introduced in this paper.

**) BCC = Beam to column contact

Fig. 8. Spring models for web angle connection with three bolt rows.

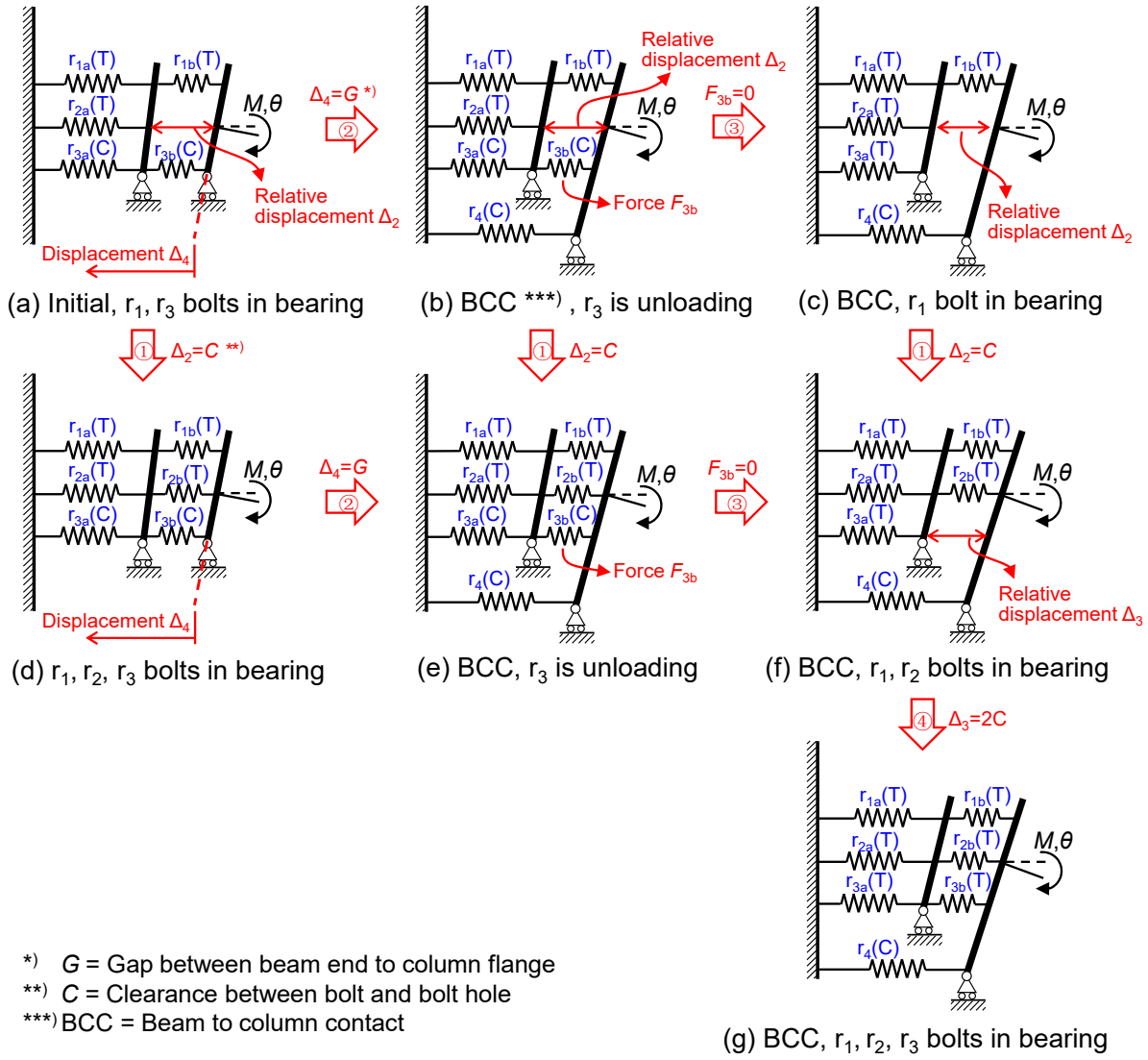

*) *G* = Gap between beam end to column flange
**) *C* = Clearance between bolt and bolt hole
***) BCC = Beam to column contact

Fig. 9. Decision tree for web angle connection spring model (three bolt rows).

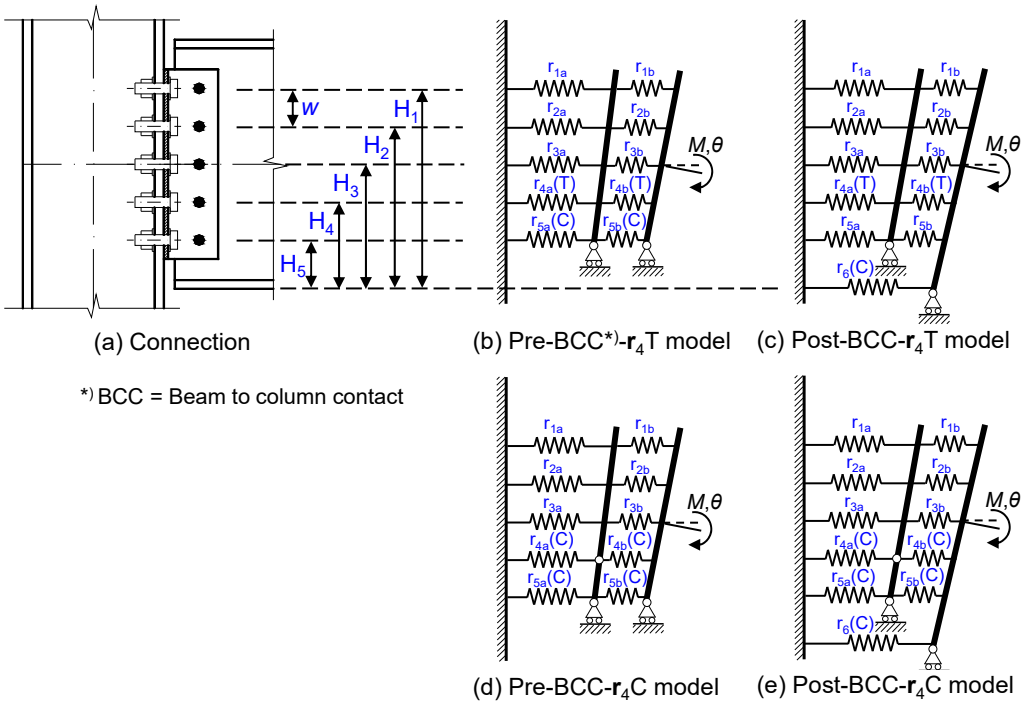

Fig. 10. Spring model for 5-bolt row web angle connection.

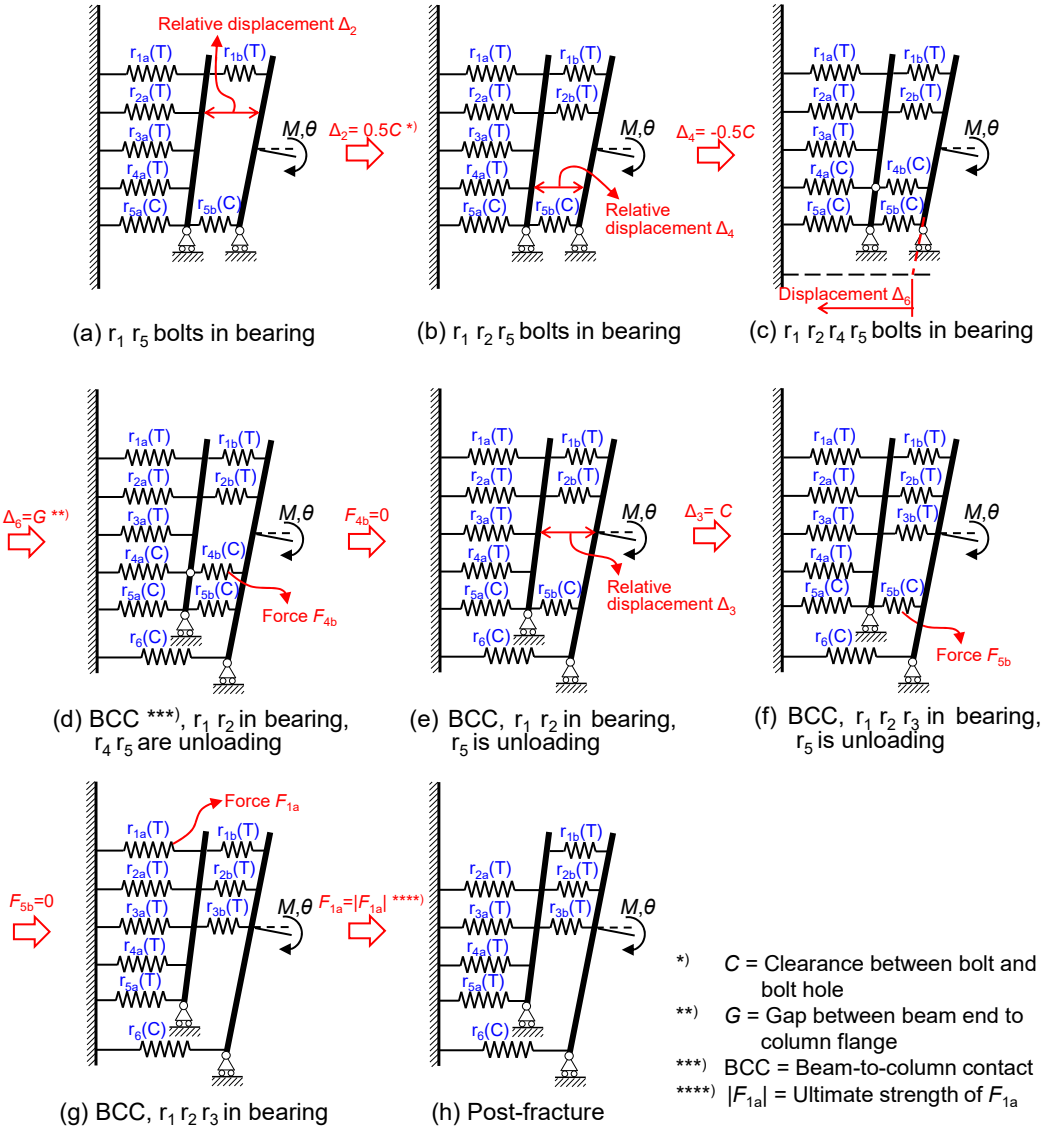

Fig. 11. Path through decision tress for WA460.

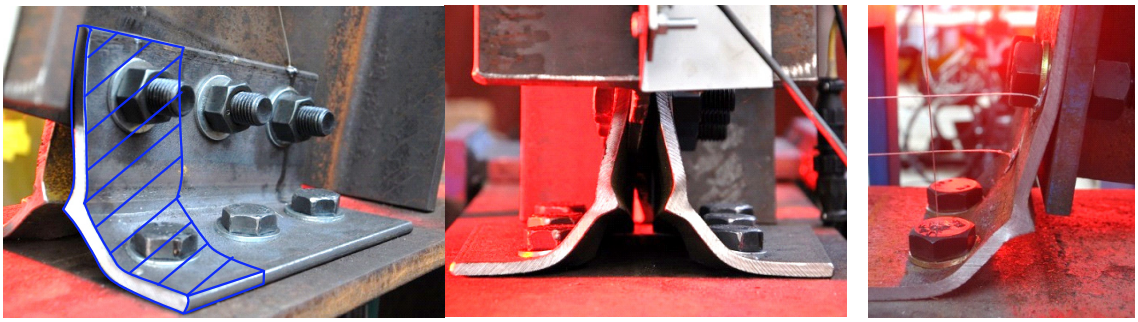

(a) Deformation of web angle (b) Flange angle deformation

Fig. 12. Analogy between web angle and top flange angle.

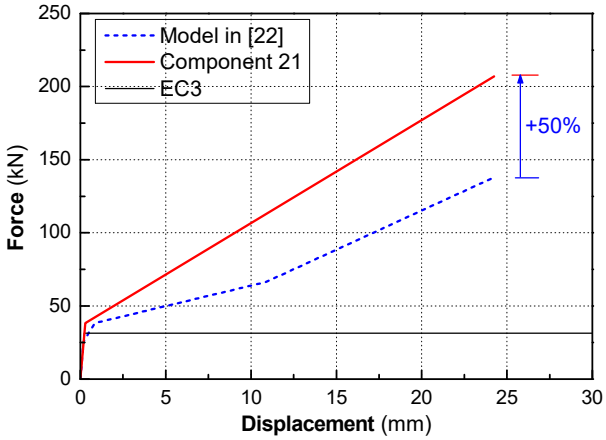

Fig. 13. Force-displacement curve of Component 21.

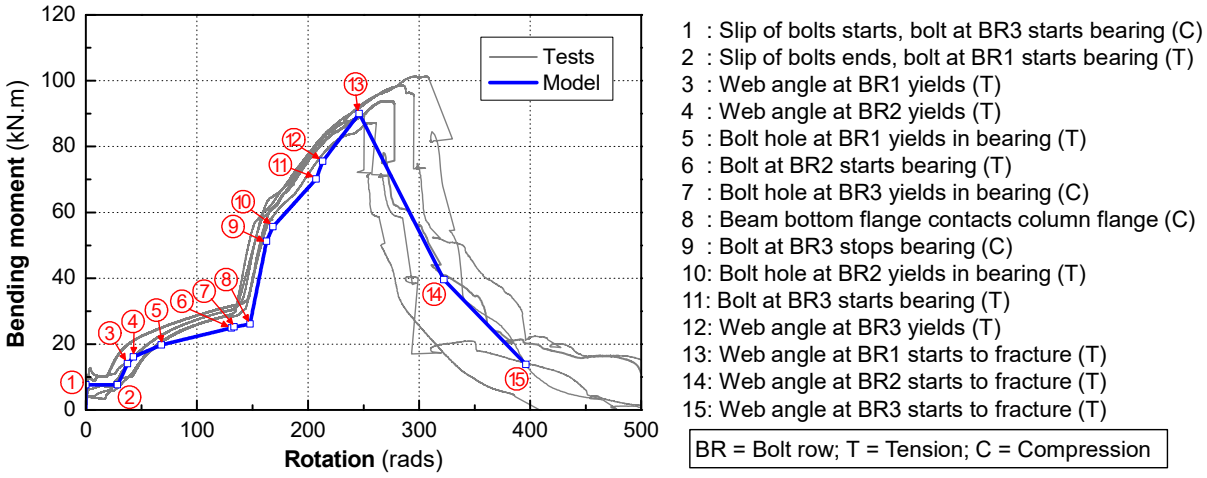

Fig. 14. Model prediction for WA360.

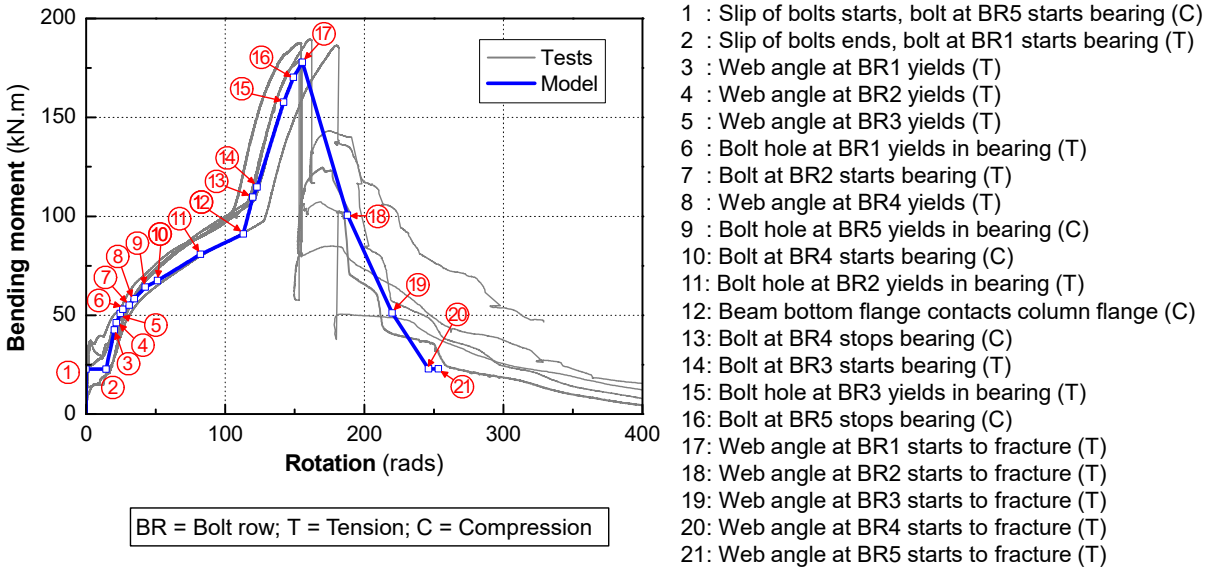

Fig. 15. Model prediction for WA460.

Table 1. Mechanical properties of specimens.

Sections	Young's Modulus (MPa)	Yield Stress (MPa)	Ultimate Tensile Strength (MPa)	Total elongation
100x100x8EA	209,400	308	444	0.31
250 UC 89.5 flange	209,900	276	448	0.40
250 UC 89.5 web	209,400	335	476	0.33
360 UB 56.7 flange	200,800	306	479	0.35
360 UB 56.7 web	209,800	336	476	0.33
460 UB 82.1 web	199,600	347	477	0.34

Table 2. Summary of WA360 series results

Specimen	Initial stage		End of Bolt slip		Beam-to-column contact		Ultimate stage		Joint ductility (mrad)
	Stiffness (kN·m/mrad)	Resistance (kN·m)	Resistance (kN·m)	Rotation (mrad)	Resistance (kN·m)	Rotation (mrad)	Resistance (kN·m)	Rotation (mrad)	
WA360-1	4.55	10.6	9.99	19.7	33.7	146	93.7	277	500
WA360-2	2.83	3.90	6.07	21.8	31.4	136	101	308	405
WA360-3	2.97	5.89	9.99	41.5	31.2	144	87.3	261	438
WA360-4	3.51	4.16	5.77	25.4	30.0	135	89.6	250	350
WA360-5	3.63	12.6	11.07	26.3	33.5	141	98.6	287	511
Average	3.50	7.44	8.58	26.9	32.0	140	94.0	277	441
SD	0.680	3.97	2.47	8.57	1.59	4.83	5.80	22.6	67.0
CoV	0.194	0.533	0.288	0.318	0.0498	0.0344	0.0617	0.0818	0.152

Table 3. Summary of WA460 series results

Specimen	Initial stage		End of Bolt slip		Beam-to-column contact		Ultimate stage		Joint ductility (mrad)
	Stiffness (kN·m/mrad)	Resistance (kN·m)	Resistance (kN·m)	Rotation (mrad)	Resistance (kN·m)	Rotation (mrad)	Resistance (kN·m)	Rotation (mrad)	
WA460-1	12.0	26.0	36.1	18.8	102	105	188	154	288
WA460-2	9.99	9.30	20.5	17.1	97.7	127	186	180	329*)
WA460-3	11.9	36.2	29.6	13.1	106	116	190	161	326
WA460-4	11.5	35.4	39.6	12.9	109	119	179	153	362
WA460-5	10.4	13.9	25.1	18.6	108	121	176	155	343
Average	11.2	24.1	30.2	16.1	105	118	184	161	330
SD	0.904	12.2	7.80	2.91	4.70	8.11	6.02	11.3	27.3
CoV	0.0809	0.507	0.259	0.1801	0.0447	0.0690	0.0327	0.0703	0.082

*) Loading was terminated when fracture in web angle propagated to the bottom bolt row; this rotation was the last recorded rotation.

Table 4. Properties of components of WA360

Spring	Component	Initial stiffness k_e (x10^{3}kN/m)	Plastic stiffness k_p (x10^{3}kN/m)	Elastic limit F_y (kN)	Ultimate strength F_u (kN)
$\mathbf{r}_{1a}$(T), $\mathbf{r}_{2a}$(T), $\mathbf{r}_{3a}$(T)	3	758	-	320	-
	4	2510	-	298	-
	10	3,643	-	441	-
	21	**137**	**7.03**	**38.3**	**207**
$\mathbf{r}_{3a}$(C)	1	1,820	-	557	-
	2	1,380	-	519	-
$\mathbf{r}_{1b}$(T), $\mathbf{r}_{2b}$(T), $\mathbf{r}_{3b}$(T)	11	800	-	294	-
	12-angle(T)	318	-	209	-
	12-web(T)	**182**	**9.1**	**86.5**	-
$\mathbf{r}_{3b}$(C)	11	800	-	294	-
	12-angle(C)	424	-	377	-
	12-web(C)	**214**	**10.7**	**127**	-
$\mathbf{r}_4$(C)	1	1,020	-	557	-
	2	1,380	-	519	-

Table 5. Properties of components of WA460

Spring	Component	Initial stiffness k_e (x10^{3}kN/m)	Plastic stiffness k_p (x10^{3}kN/m)	Elastic limit F_y (kN)	Ultimate strength F_u (kN)
$\mathbf{r}_{1a}$(T), $\mathbf{r}_{2a}$(T), $\mathbf{r}_{3a}$(T), $\mathbf{r}_{4a}$(T), $\mathbf{r}_{5a}$(T)	3	758	-	320	-
	4	2510	-	298	-
	10	3,643	-	441	-
	21	**137**	**7.03**	**38.3**	**207**
$\mathbf{r}_{4a}$(C)	1	1,220	-	557	-
	2	1,380	-	519	-
$\mathbf{r}_{5a}$(C)	1	912	-	557	-
	2	1,380	-	519	-
$\mathbf{r}_{1b}$(T), $\mathbf{r}_{2b}$(T), $\mathbf{r}_{3b}$(T), $\mathbf{r}_{4b}$(T), $\mathbf{r}_{5b}$(T)	11	800	-	294	-
	12-angle(T)	318	-	209	-
	12-web(T)	**225**	**11.3**	**107**	-
$\mathbf{r}_{4b}$(C) $\mathbf{r}_{5b}$(C)	11	800	-	294	-
	12-angle(C)	424	-	377	-
	12-web(C)	**265**	**13.3**	**157**	-
$\mathbf{r}_6$(C)	1	690	-	557	-
	2	1,380	-	519	-